Size-dependent nonlinear secondary resonance of micro/nano-beams made of nanoporous biomaterials including truncated cube cells

Saeid Sahmani[a*], Mohamad Fotouhi[b], Mohammad Mohammadi Aghdam[c]

[a] *Mechanical Rotating Equipment Department, Niroo Research Institute (NRI), Tehran 16656-517, Iran*
[b] *Design and Mathematics Department, University of the West England, Bristol BS16 1QY, UK*
[c] *Mechanical Engineering Department, Amirkabir University of Technology, Tehran 15875-4413, Iran*

Abstract

Porous biomaterials have been utilized in cellular structures in order to mimic the function of bone as a branch of tissue engineering approach. With the aid of nanoporous biomaterials in which the pore size is at nanoscale, the capability of biological molecular isolation becomes more efficient. In the present study, firstly the mechanical properties of nanoporous biomaterials are estimated on the basis of a truncated cube cell model including a refined hyperbolic shear deformation for the associated lattice structure. After that, based upon a nonlocal strain gradient beam model, the size-dependent nonlinear secondary resonance of micro/nano-beams made of the nanoporous biomaterial is predicted corresponding to the both of subharmonic and superharmonic excitations. The non-classical governing differential equation of motion is constructed via Hamilton's principle. By employing the Galerkin technique together with the multiple time-scales method, the nonlocal strain gradient frequency-response and amplitude-response of the nonlinear oscillation of micro/nano-beams made of a nanoporous biomaterial under hard excitation are achieved. It is shown that in the superharmonic case, increasing the pore size leads to enhance the nonlinear hardening spring-type behavior of jump phenomenon and the height of limit point bifurcations. In the subharmonic case, higher pore size causes to increase the gap between two branches associated with the high-frequency and low-frequency solutions.

Keywords: Nano-biomechanics; Porosity; Nonlinear oscillation; Size dependency; Nonlocal strain gradient theory.

[*]Corresponding author. Tel.: +98 21 66405844, Fax: +98 21 66419736.
E-mail address: sahmani@aut.ac.ir (S. Sahmani).

1. Introduction

Biomaterials have the capability to use in making structures to replace a part or a function of a living organism in a reliable way without adversely affecting it. In order to display tissue formation more efficiently, porous biomaterials are utilized which allow proliferation and vascularization of a living cell as well as interlocking between the biomaterial and surrounding natural tissue.

By rapid advancement in science and technology, more effective methods to deliver and release drug into the body have been determined. Using porous nanostructures in one of these efficient ways for controlling the delivery of the drug [1-3]. Having high surface area with several pores makes porous nanostructures as an ideal candidate for the encapsulation of pharmaceutical drugs [4]. Also, vibration analysis is an important study in biomedical applications. For instance, Usui et al. [5] investigated radiographically and biomechanically the effects of mechanical vibration on bone ingrowth into porous hydroxyapatite implants and fracture healing in a rabbit model. Altintas [6] performed a modal vibration analysis of a heterogeneous porous structure by taking microstructural details into consideration.

Through miniaturizing a solid material to nanoscale, size dependency characteristics take on an importance which is normally inconsequential at usual scale. This size induced property change has inspired to develop several size-dependent continuum theories such as nonlocal elasticity theory [7], surface elasticity theory [8], strain gradient elasticity theory [9], and couple stress elasticity theory [10]. In recent years, variety of studies have been conducted to employ these non-classical continuum theories of elasticity to investigate crucial characteristics of mechanical response of nanostructures [11-51].

Recently, Lim et al. [52] introduced a refined nonlocal continuum mechanics namely as nonlocal strain gradient elasticity theory including simultaneously the both of hardening-stiffness and softening-stiffness of size effect. After that, some studies have been carried out to construct the integral elasticity type of this theory [53,54]. In recent years, the newly proposed elasticity theory has been widely utilized to capture stress and strain gradient scaling effects on mechanical behavior of micro/nano-structures. Tang et al. [55] developed a nonlocal strain gradient Timoshenko beam model for wave dispersion in a viscoelastic single-walled carbon nanotube. Li et al. [56] analyzed bending, buckling and vibration of axially functionally graded nanobeams on the basis of nonlocal strain gradient elasticity theory. Ebrahimi and Dabbagh [57] predicted the flexural wave propagation of functionally graded magneto-electro-elastic nanoplates based upon the nonlocal strain gradient theory of elasticity. Sahmani and Aghdam [58] employed nonlocal strain gradient elasticity theory to analyze the nonlinear instability of axially loaded microtubules surrounded of cytoplasm of a living cell. Lu et al. [59] explored the size-dependent free vibrations of nanobeams by incorporating the nonlocal strain gradient theory to the sinusoidal shear deformation beam theory. Sahmani and Aghdam [60] constructed a nonlocal strain gradient shell model to anticipate buckling and postbuckling behavior of axially loaded multilayer functionally graded nanoshells reinforced with graphene platelets. Zhu and Li [61] proposed a closed form solution based upon nonlocal strain gradient elasticity theory for a small-scaled rod in tension. Sahmani and Aghdam [62] used the nonlocal strain gradient continuum mechanics to examine the nonlinear instability of hydrostatic pressurized multilayer functionally graded nanoshells reinforced with graphene nanoplatelets. Li and Hu [63] investigated the size-dependent postbuckling behavior of functionally graded nanobeams including nanlocality and strain gradient size dependency. Sahmani and Aghdam [64] constructed a nonlocal strain gradient higher-order shear deformable beam model for nonlinear vibration analysis of postbuckling multilayer functionally graded nanobeams. They also predicted the nonlinear primary resonance of a nanobeam made of nanoorous biomaterial subjected to soft excitation [65]. Radwan and Sobhy [66] developed a nonlocal strain gradient plate model for dynamic deformation of viscoelastic graphene nanosheets under harmonic thermal load. Sahmani et al. [67-69] analyzed the size-dependent nonlinear mechanical behaviors of reinforced functionally graded porous micro/nano-structures on the basis of the nonlocal strain gradient theory of elasticity. Recently, Li et al. [70] investigated the influence of the beam thickness on the size-dependent buckling and postbuckling characteristics of nanobeams modeled via the nonlocal strain gradient theory.

The objective of this work is to predict the size-dependent nonlinear secondary resonance of a micro/nano-beam made of nanoporous biomaterials including truncated cubic unit cells. To accomplish this purpose, the mechanical properties of the nanoporous biomaterial comprising the truncated cube cells including a refined hyperbolic shear deformation effect are obtained analytical as functions of the pore size. After that, based on the nonlocal strain gradient elasticity theory, a size-dependent beam model is constructed. By using the Galerkin technique together with the multiple time-scales method, analytical expressions for the frequency-response and amplitude-response of a micro/nano-beam made of the nanoporous biomaterial are proposed for the both of subharmonic and superharmonic excitations.

2. Analytical approach for mechanical properties of nanoporous biomaterials

In order to simulate a nanoporous biomaterial, it is supposed that it is comprised of truncated cube cells (open cell foam) as depicted in Figure 1. As a consequent, by placing these cubes beside each other, a unit cell is created. Consequently, the model consists of bigger truncated cube cells and smaller octahedral cells. It is shown in Figure 2 that because of the geometrical symmetry, the links $c_1a_1b_1d_1a_2c_2$ and $c_1a_1b_2d_2a_2c_2$ and $c_1a_1b_3d_3a_2c_2$ and $c_1a_1b_4d_4a_2c_2$ of the unit cell have the same mechanical in-plane deformations. Therefore, it is enough to analyze one of them in order to anticipate the mechanical characteristics of the unit cell. In the current study, the link $c_1a_1b_1d_1a_2c_2$ is selected to be analyzed.

On the basis of the refined hyperbolic shear deformable beam model related to the links of the unit cell, it yields

$$\bar{E}\bar{I}\frac{d^4w}{dx^4} = \bar{E}\bar{I}\left[\cosh\left(\frac{1}{2}\right) - 12\left(\cosh\left(\frac{1}{2}\right) - 2\sinh\left(\frac{1}{2}\right)\right)\right]\frac{d^3\psi}{dx^3} + q(x) \tag{1a}$$

$$\bar{E}\bar{I}\left[\cosh\left(\frac{1}{2}\right) - 12\left(\cosh\left(\frac{1}{2}\right) - 2\sinh\left(\frac{1}{2}\right)\right)\right]\frac{d^3w}{dx^3}$$
$$= \bar{E}\bar{I}\left[\left(\cosh\left(\frac{1}{2}\right)\right)^2 + 6(\sinh(1) - 1) - 24\cosh\left(\frac{1}{2}\right)\left(\cosh\left(\frac{1}{2}\right) - 2\sinh\left(\frac{1}{2}\right)\right)\right]\frac{d^2\psi}{dx^2}$$
$$- \bar{G}\bar{A}\left[\left(\cosh\left(\frac{1}{2}\right)\right)^2 + \frac{1}{2}(\sinh(1) + 1) - 4\cosh\left(\frac{1}{2}\right)\sinh\left(\frac{1}{2}\right)\right]\psi \qquad (1b)$$

where $\bar{E}, \bar{G}, \bar{I}, \bar{A}, w, \psi$ represent, respectively, the Young's modulus, shear modulus, moment inertia, cross-section area, deflection and angle of rotation for the links of unit cell.

Consequently, for a cantilever beam with constructed load P at the free end and length of ℓ, one will have

$$\delta_p = w(\ell) = \frac{P\ell^3}{3\bar{E}\bar{I}} + \frac{6}{5}\frac{P\ell}{\bar{G}\bar{A}}\left(1 + \frac{\cosh(\wp\ell) - \sinh(\wp\ell) - 1}{\wp\ell}\right) \qquad (2a)$$

$$\theta = \varphi(\ell) = \frac{P\ell^2}{2\bar{E}\bar{I}} + \frac{6}{5}\frac{P}{\bar{G}\bar{A}}(1 + \sinh(\wp\ell) - \cosh(\wp\ell)) \qquad (2b)$$

where

$$\wp = \sqrt{\frac{\frac{\bar{G}\bar{A}}{\bar{E}\bar{I}}\frac{\varsigma_3}{\varsigma_1}}{\frac{\varsigma_2}{\varsigma_1} - \varsigma_1}} \qquad (3)$$

$$\varsigma_1 = \cosh\left(\frac{1}{2}\right) - 12\left[\cosh\left(\frac{1}{2}\right) - 2\sinh\left(\frac{1}{2}\right)\right] \qquad (4a)$$

$$\varsigma_2 = \left(\cosh\left(\frac{1}{2}\right)\right)^2 + 6[\sinh(1) - 1] - 24\cosh\left(\frac{1}{2}\right)\left[\cosh\left(\frac{1}{2}\right) - 2\sinh\left(\frac{1}{2}\right)\right] \qquad (4b)$$

$$\varsigma_3 = \left(\cosh\left(\frac{1}{2}\right)\right)^2 + \frac{1}{2}[\sinh(1) + 1] - 4\cosh\left(\frac{1}{2}\right)\sinh\left(\frac{1}{2}\right) \qquad (4c)$$

Based upon the hyperbolic shear deformation beam theory, it is supposed that for the in-plane and transverse displacements, the bending components do not contribute toward shear components and vice versa. Also, there is no need to a shear correction factor which is hard to find its value as it depends on various parameters.

As a result, the equivalent bending moment at the free end of the strut causing the same rotation can be obtained as

$$\frac{P\ell^2}{2\bar{E}\bar{I}} + \frac{6}{5}\frac{P}{\bar{G}\bar{A}}(1 + \sinh(\wp\ell) - \cosh(\wp\ell)) = \frac{M\ell}{\bar{E}\bar{I}} \to M$$
$$= \frac{P\ell}{2} + \frac{6}{5}\frac{P\bar{E}\bar{I}}{\ell\bar{G}\bar{A}}(1 + \sinh(\wp\ell) - \cosh(\wp\ell)) \qquad (5)$$

The associated lateral deflection caused by applying the both concentrated load P and bending moment M at the free end can written as

$$\delta = \delta_P + \delta_M = \frac{P\ell^3}{3\bar{E}\bar{I}} + \frac{6}{5}\frac{P\ell}{\bar{G}\bar{A}}\left(1 + \frac{\cosh(\wp\ell) - \sinh(\wp\ell) - 1}{\wp\ell}\right)$$
$$- \left[\frac{P\ell}{2} + \frac{6}{5}\frac{P\bar{E}\bar{I}}{\ell\bar{G}\bar{A}}(1 + \sinh(\wp\ell) - \cosh(\wp\ell))\right]\frac{\ell^2}{2\bar{E}\bar{I}}$$
$$= \frac{P\ell^3}{12\bar{E}\bar{I}} + \frac{3}{5}\frac{P\ell}{\bar{G}\bar{A}} + \frac{6}{5}\frac{P\ell}{\bar{G}\bar{A}}\left(\frac{\left(1 + \frac{\wp\ell}{2}\right)\cosh(\wp\ell) - \left(1 + \frac{\wp\ell}{2}\right)\sinh(\wp\ell) - 1}{\wp\ell}\right) \tag{6}$$

So, one will have

$$P = \frac{\delta}{\frac{\ell^3}{12\bar{E}\bar{I}} + \frac{3\ell}{5\bar{G}\bar{A}} + \frac{6}{5\bar{G}\bar{A}}\left(\frac{\left(1 + \frac{\wp\ell}{2}\right)\cosh(\wp\ell) - \left(1 + \frac{\wp\ell}{2}\right)\sinh(\wp\ell) - 1}{\wp}\right)} \tag{7}$$

In a general view, the in-plane deformation causes 18 degrees of freedom for the link $c_1a_1b_1d_1a_2c_2$. Nevertheless, the following reasonable assumptions similar to those considered by Hedayati et al [71] are taken into account in order to decrease the number of degrees of freedom to 6 as illustrated in Figure 3:

- All of the vertices of links do not enable to rotate
- The points a_1, a_2, c_1 enable only to displace vertically
- The points b_1 and d_1 displace the same vertically, but different horizontally.
- The point c_2 is fixed.

Moreover, it is assumed that the porosity is distributed uniformly in the biomaterial, and its shape is similar in all points of the biomaterial.

Consequently, the relationships between the degrees of freedom $\varkappa_i$ $(i = 1,2, \dots ,6)$ and the associated external force S_i $(i = 1,2, \dots ,6)$ can be expressed as

$$\begin{Bmatrix} S_1 \\ S_2 \\ S_3 \\ S_4 \\ S_5 \\ S_6 \end{Bmatrix} = \begin{bmatrix} \mathcal{K}_{11} & \mathcal{K}_{12} & \mathcal{K}_{13} & \mathcal{K}_{14} & \mathcal{K}_{15} & \mathcal{K}_{16} \\ \mathcal{K}_{21} & \mathcal{K}_{22} & \mathcal{K}_{23} & \mathcal{K}_{24} & \mathcal{K}_{25} & \mathcal{K}_{26} \\ \mathcal{K}_{31} & \mathcal{K}_{32} & \mathcal{K}_{33} & \mathcal{K}_{34} & \mathcal{K}_{35} & \mathcal{K}_{36} \\ \mathcal{K}_{41} & \mathcal{K}_{42} & \mathcal{K}_{43} & \mathcal{K}_{44} & \mathcal{K}_{45} & \mathcal{K}_{46} \\ \mathcal{K}_{51} & \mathcal{K}_{52} & \mathcal{K}_{53} & \mathcal{K}_{54} & \mathcal{K}_{55} & \mathcal{K}_{56} \\ \mathcal{K}_{61} & \mathcal{K}_{62} & \mathcal{K}_{63} & \mathcal{K}_{64} & \mathcal{K}_{65} & \mathcal{K}_{66} \end{bmatrix} \begin{Bmatrix} \varkappa_1 \\ \varkappa_2 \\ \varkappa_3 \\ \varkappa_4 \\ \varkappa_5 \\ \varkappa_6 \end{Bmatrix} \tag{8}$$

Through expression of the displacements corresponding to each degree of freedom separately in such a way that the considered degree of freedom is supposed to be unit and the other ones are assumed to be zero, the elements of the stiffness matrix can be extracted column by column.

For $\varkappa_1 = 1$ and $\varkappa_2 = \varkappa_3 = \varkappa_4 = \varkappa_5 = \varkappa_6 = 0$:

As a result, the point c_1 displaces downwards by unity. The following associated forces in the struts can be achieved

$$S_1 = \frac{2\bar{A}\bar{E}}{\ell} \quad , \quad S_2 = -\frac{2\bar{A}\bar{E}}{\ell} \quad , \quad S_3 = S_4 = S_5 = S_6 = 0 \tag{9}$$

For $\varkappa_2 = 1$ and $\varkappa_1 = \varkappa_3 = \varkappa_4 = \varkappa_5 = \varkappa_6 = 0$:

As a result, the point a_1 (the vertices of links $a_1b_1, a_1b_2, a_1b_3, a_1b_4$) displaces downwards by unity. The following associated forces in the struts can be achieved

$$S_1 = -\frac{2\bar{A}\bar{E}}{\ell} \quad , \quad S_4 = S_6 = 0$$

$$S_2 = \frac{2\bar{A}\bar{E}}{\ell} + 4 \times \left(\frac{1}{\frac{\ell^3}{6\bar{E}\bar{I}} + \frac{6\ell}{5\bar{G}\bar{A}} + \frac{12}{5\bar{G}\bar{A}} \left(\frac{\left(1 + \frac{\wp\ell}{2}\right)\cosh(\wp\ell) - \left(1 + \frac{\wp\ell}{2}\right)\sinh(\wp\ell) - 1}{\wp} \right)} + \frac{\bar{A}\bar{E}}{2\ell} \right)$$

$$S_3 = -4 \times \left(\frac{1}{\frac{\ell^3}{6\bar{E}\bar{I}} + \frac{6\ell}{5\bar{G}\bar{A}} + \frac{12}{5\bar{G}\bar{A}} \left(\frac{\left(1 + \frac{\wp\ell}{2}\right)\cosh(\wp\ell) - \left(1 + \frac{\wp\ell}{2}\right)\sinh(\wp\ell) - 1}{\wp} \right)} + \frac{\bar{A}\bar{E}}{2\ell} \right) \tag{10}$$

$$S_5 = 4 \times \left(\frac{1}{\frac{\ell^3}{6\bar{E}\bar{I}} + \frac{6\ell}{5\bar{G}\bar{A}} + \frac{12}{5\bar{G}\bar{A}} \left(\frac{\left(1 + \frac{\wp\ell}{2}\right)\cosh(\wp\ell) - \left(1 + \frac{\wp\ell}{2}\right)\sinh(\wp\ell) - 1}{\wp} \right)} - \frac{\bar{A}\bar{E}}{2\ell} \right)$$

For $\varkappa_3 = 1$ and $\varkappa_1 = \varkappa_2 = \varkappa_4 = \varkappa_5 = \varkappa_6 = 0$:

As a result, the point b_1 (similarly, the points b_2, b_3, b_4) displaces downwards by unity. The associated forces in the struts become

$$S_1 = S_5 = S_6 = 0$$

$$S_2 = S_4 = -4 \times \left(\frac{1}{\frac{\ell^3}{6\bar{E}\bar{I}} + \frac{6\ell}{5\bar{G}\bar{A}} + \frac{12}{5\bar{G}\bar{A}} \left(\frac{\left(1 + \frac{\wp\ell}{2}\right)\cosh(\wp\ell) - \left(1 + \frac{\wp\ell}{2}\right)\sinh(\wp\ell) - 1}{\wp} \right)} - \frac{\bar{A}\bar{E}}{2\ell} \right) \tag{11}$$

$$S_3 = 4 \times \left(\frac{1}{\frac{\ell^3}{12\bar{E}\bar{I}} + \frac{3\ell}{5\bar{G}\bar{A}} + \frac{6}{5\bar{G}\bar{A}}\left(\frac{\left(1+\frac{p\ell}{2}\right)\cosh(p\ell) - \left(1+\frac{p\ell}{2}\right)\sinh(p\ell) - 1}{p} \right)} + \frac{\bar{A}\bar{E}}{\ell} \right)$$

For $\varkappa_4 = 1$ and $\varkappa_1 = \varkappa_2 = \varkappa_3 = \varkappa_5 = \varkappa_6 = 0$:

As a result, the point a_2 (the vertices of links $a_2b_1, a_2b_2, a_2b_3, a_2b_4$) displaces downwards by unity. The associated forces in the struts are as below

$S_1 = S_2 = S_6 = 0$

$$S_3 = -4 \times \left(\frac{1}{\frac{\ell^3}{6\bar{E}\bar{I}} + \frac{6\ell}{5\bar{G}\bar{A}} + \frac{12}{5\bar{G}\bar{A}}\left(\frac{\left(1+\frac{p\ell}{2}\right)\cosh(p\ell) - \left(1+\frac{p\ell}{2}\right)\sinh(p\ell) - 1}{p} \right)} + \frac{\bar{A}\bar{E}}{2\ell} \right) \tag{12}$$

$$S_4 = \frac{2\bar{A}\bar{E}}{\ell} + 4 \times \left(\frac{1}{\frac{\ell^3}{6\bar{E}\bar{I}} + \frac{6\ell}{5\bar{G}\bar{A}} + \frac{12}{5\bar{G}\bar{A}}\left(\frac{\left(1+\frac{p\ell}{2}\right)\cosh(p\ell) - \left(1+\frac{p\ell}{2}\right)\sinh(p\ell) - 1}{p} \right)} + \frac{\bar{A}\bar{E}}{2\ell} \right)$$

$$S_5 = -4 \times \left(\frac{1}{\frac{\ell^3}{6\bar{E}\bar{I}} + \frac{6\ell}{5\bar{G}\bar{A}} + \frac{12}{5\bar{G}\bar{A}}\left(\frac{\left(1+\frac{p\ell}{2}\right)\cosh(p\ell) - \left(1+\frac{p\ell}{2}\right)\sinh(p\ell) - 1}{p} \right)} - \frac{\bar{A}\bar{E}}{2\ell} \right)$$

For $\varkappa_5 = 1$ and $\varkappa_1 = \varkappa_2 = \varkappa_3 = \varkappa_4 = \varkappa_6 = 0$:

As a result, the point b_1 (similarly, the points b_2, b_3, b_4) displaces horizontally by unity. The associated forces in the struts can be given as

$S_1 = S_3 = 0$

$$S_2 = 4 \times \left(\frac{1}{\frac{\ell^3}{6\bar{E}\bar{I}} + \frac{6\ell}{5\bar{G}\bar{A}} + \frac{12}{5\bar{G}\bar{A}}\left(\frac{\left(1+\frac{p\ell}{2}\right)\cosh(p\ell) - \left(1+\frac{p\ell}{2}\right)\sinh(p\ell) - 1}{p} \right)} - \frac{\bar{A}\bar{E}}{2\ell} \right)$$

$$S_4 = -4 \times \left(\frac{1}{\frac{\ell^3}{6\bar{E}\bar{I}} + \frac{6\ell}{5\bar{G}\bar{A}} + \frac{12}{5\bar{G}\bar{A}}\left(\frac{\left(1+\frac{\wp\ell}{2}\right)\cosh(\wp\ell) - \left(1+\frac{\wp\ell}{2}\right)\sinh(\wp\ell) - 1}{\wp} \right)} - \frac{\bar{A}\bar{E}}{2\ell} \right) \tag{13}$$

$$S_5 = 4 \times \left(\frac{1}{\frac{\ell^3}{12\bar{E}\bar{I}} + \frac{3\ell}{5\bar{G}\bar{A}} + \frac{6}{5\bar{G}\bar{A}}\left(\frac{\left(1+\frac{\wp\ell}{2}\right)\cosh(\wp\ell) - \left(1+\frac{\wp\ell}{2}\right)\sinh(\wp\ell) - 1}{\wp} \right)} + \frac{5\bar{A}\bar{E}}{\ell} \right)$$

$$S_6 = -4 \times \left(\frac{2\bar{A}\bar{E}}{\ell} \right)$$

For $\varkappa_6 = 1$ and $\varkappa_1 = \varkappa_2 = \varkappa_3 = \varkappa_4 = \varkappa_5 = 0$:

As a result, the point d_1 (similarly, the points d_2, d_3, d_4) displaces horizontally by unity. The associated forces in the struts can be expressed as:

$$S_1 = S_2 = S_3 = S_4 = 0$$

$$S_5 = -4\left(\frac{2\bar{A}\bar{E}}{\ell}\right) \tag{14}$$

$$S_6 = 4\left(\frac{2\bar{A}\bar{E}}{\ell}\right)$$

Following equation (8) leads to the elements of the stiffness matrix which are given in Appendix A.

As it was mentioned by Hedayati et al. [71], it is assumed that the external force, P, acts vertically on point c_1 of the refined truncated cube lattice structure, which causes an additional horizontal force equal to $\frac{8\bar{A}\bar{E}(\varkappa_6-\varkappa_5)}{\ell}$ at point d_1. Therefore, it yields

$$\begin{Bmatrix} P \\ 0 \\ 0 \\ 0 \\ 0 \\ 0 \end{Bmatrix} = \begin{bmatrix} \mathcal{K}_{11} & \mathcal{K}_{12} & 0 & 0 & 0 & 0 \\ \mathcal{K}_{21} & \mathcal{K}_{22} & \mathcal{K}_{23} & 0 & \mathcal{K}_{25} & 0 \\ 0 & \mathcal{K}_{32} & \mathcal{K}_{33} & \mathcal{K}_{34} & 0 & 0 \\ 0 & 0 & \mathcal{K}_{43} & \mathcal{K}_{44} & \mathcal{K}_{45} & 0 \\ 0 & \mathcal{K}_{52} & 0 & \mathcal{K}_{54} & \mathcal{K}_{55} & \mathcal{K}_{56} \\ 0 & 0 & 0 & 0 & 2\mathcal{K}_{65} & 2\mathcal{K}_{66} \end{bmatrix} \begin{Bmatrix} \varkappa_1 \\ \varkappa_2 \\ \varkappa_3 \\ \varkappa_4 \\ \varkappa_5 \\ \varkappa_6 \end{Bmatrix} \tag{15}$$

This point should be noted that a simpler version of the unit cell used here in the lattice structure of porous materials has been studied previously by Sun et al. [72] and Yang [73], in which the horizontal struts (struts $b_1b_2, b_2b_3, b_3b_4, b_4b_1$ shown in Figure 2) as important factors in the structure strength are excluded. The presence of this horizontal struts has the advantage to make an approximately isotropic homogenization for the lattice structure. Consequently, as it is depicted in Figure 3 for an instance, the links of the present unit cell in the lattice structure are geometrically similar (the square $b_1b_2b_3b_4$ is the symmetric plane of the unit cell). Consequently, the elastic modulus of the truncated cube unit cell can be calculated as:

$$E=\frac{F_uL_u}{A_u\delta_u}=\frac{P}{(1+\sqrt{2})\ell\varkappa_1} \tag{16}$$

where F_u, L_u, A_u, δ_u denote, respectively, the applied load, length, cross-sectional area, and shortening of the unit cell.

After that, inversion of equation (16) results in $\varkappa_1$ as a function of P. Therefore, after some mathematical calculations, it can be written

$$\begin{aligned}E = (&\mathcal{K}_{11}\mathcal{K}_{22}\mathcal{K}_{33}\mathcal{K}_{66}\mathcal{K}_{45}\mathcal{K}_{54} - \mathcal{K}_{11}\mathcal{K}_{22}\mathcal{K}_{33}\mathcal{K}_{44}\mathcal{K}_{55}\mathcal{K}_{66} + \mathcal{K}_{11}\mathcal{K}_{22}\mathcal{K}_{55}\mathcal{K}_{66}\mathcal{K}_{34}\mathcal{K}_{43} \\ &+ \mathcal{K}_{11}\mathcal{K}_{33}\mathcal{K}_{44}\mathcal{K}_{66}\mathcal{K}_{25}\mathcal{K}_{52} - \mathcal{K}_{11}\mathcal{K}_{66}\mathcal{K}_{25}\mathcal{K}_{52}\mathcal{K}_{34}\mathcal{K}_{43} + 2\mathcal{K}_{11}\mathcal{K}_{66}\mathcal{K}_{34}\mathcal{K}_{45}\mathcal{K}_{23}\mathcal{K}_{25} \\ &+ \mathcal{K}_{11}\mathcal{K}_{44}\mathcal{K}_{55}\mathcal{K}_{66}\mathcal{K}_{23}\mathcal{K}_{32} - \mathcal{K}_{11}\mathcal{K}_{66}\mathcal{K}_{45}\mathcal{K}_{54}\mathcal{K}_{23}\mathcal{K}_{32} + \mathcal{K}_{33}\mathcal{K}_{44}\mathcal{K}_{55}\mathcal{K}_{66}\mathcal{K}_{12}\mathcal{K}_{21} \\ &- \mathcal{K}_{33}\mathcal{K}_{66}\mathcal{K}_{45}\mathcal{K}_{54}\mathcal{K}_{12}\mathcal{K}_{21} - \mathcal{K}_{55}\mathcal{K}_{66}\mathcal{K}_{12}\mathcal{K}_{21}\mathcal{K}_{34}\mathcal{K}_{43} + \mathcal{K}_{11}\mathcal{K}_{22}\mathcal{K}_{33}\mathcal{K}_{44}\mathcal{K}_{56}\mathcal{K}_{65} \\ &- \mathcal{K}_{33}\mathcal{K}_{44}\mathcal{K}_{12}\mathcal{K}_{21}\mathcal{K}_{56}\mathcal{K}_{65} - \mathcal{K}_{11}\mathcal{K}_{44}\mathcal{K}_{23}\mathcal{K}_{32}\mathcal{K}_{56}\mathcal{K}_{65} - \mathcal{K}_{11}\mathcal{K}_{22}\mathcal{K}_{34}\mathcal{K}_{43}\mathcal{K}_{56}\mathcal{K}_{65} \\ &+ \mathcal{K}_{12}\mathcal{K}_{21}\mathcal{K}_{34}\mathcal{K}_{43}\mathcal{K}_{56}\mathcal{K}_{65}) \\ &/\big[(\mathcal{K}_{66}\mathcal{K}_{22}\mathcal{K}_{33}\mathcal{K}_{45}\mathcal{K}_{54} - \mathcal{K}_{66}\mathcal{K}_{22}\mathcal{K}_{33}\mathcal{K}_{55}\mathcal{K}_{44} + \mathcal{K}_{22}\mathcal{K}_{55}\mathcal{K}_{66}\mathcal{K}_{34}\mathcal{K}_{43} \\ &+ \mathcal{K}_{33}\mathcal{K}_{44}\mathcal{K}_{66}\mathcal{K}_{25}\mathcal{K}_{52} - \mathcal{K}_{66}\mathcal{K}_{25}\mathcal{K}_{52}\mathcal{K}_{34}\mathcal{K}_{43} + 2\mathcal{K}_{66}\mathcal{K}_{45}\mathcal{K}_{34}\mathcal{K}_{23}\mathcal{K}_{25} \\ &+ \mathcal{K}_{44}\mathcal{K}_{55}\mathcal{K}_{66}\mathcal{K}_{23}\mathcal{K}_{32} - \mathcal{K}_{66}\mathcal{K}_{45}\,\mathcal{K}_{54}\mathcal{K}_{23}\mathcal{K}_{32} + \mathcal{K}_{22}\mathcal{K}_{33}\mathcal{K}_{44}\mathcal{K}_{56}\mathcal{K}_{65} \\ &- \mathcal{K}_{44}\mathcal{K}_{23}\mathcal{K}_{32}\mathcal{K}_{56}\mathcal{K}_{65} - \mathcal{K}_{22}\mathcal{K}_{34}\mathcal{K}_{43}\mathcal{K}_{56}\mathcal{K}_{65})(1+\sqrt{2})\ell\big]\end{aligned} \tag{17}$$

In addition, to capture the Poisson's ratio of the nanoporous biomaterial, it can be defined as the ratio of horizontal to vertical displacements pf the unit cell as follows

$$\nu=\frac{2\varkappa_6}{\varkappa_1} \tag{18}$$

Therefore, it can be rewritten as

$$\begin{aligned}\nu = 2&\mathcal{K}_{12}\mathcal{K}_{56}(\mathcal{K}_{33}\mathcal{K}_{44}\mathcal{K}_{25} - \mathcal{K}_{25}\mathcal{K}_{34}\mathcal{K}_{43} + \mathcal{K}_{23}\mathcal{K}_{34}\mathcal{K}_{45}) \\ &/(\mathcal{K}_{22}\mathcal{K}_{33}\mathcal{K}_{66}\mathcal{K}_{45}\mathcal{K}_{54} - \mathcal{K}_{22}\mathcal{K}_{33}\mathcal{K}_{44}\mathcal{K}_{55}\mathcal{K}_{66} + \mathcal{K}_{22}\mathcal{K}_{55}\mathcal{K}_{66}\mathcal{K}_{34}\mathcal{K}_{43} \\ &+ \mathcal{K}_{33}\mathcal{K}_{44}\mathcal{K}_{66}\mathcal{K}_{25}\mathcal{K}_{52} - \mathcal{K}_{66}\mathcal{K}_{25}\mathcal{K}_{52}\mathcal{K}_{34}\mathcal{K}_{43} + 2\mathcal{K}_{66}\mathcal{K}_{23}\mathcal{K}_{25}\mathcal{K}_{34}\mathcal{K}_{45} \\ &+ \mathcal{K}_{44}\mathcal{K}_{55}\mathcal{K}_{66}\mathcal{K}_{23}\mathcal{K}_{32} - \mathcal{K}_{66}\mathcal{K}_{23}\mathcal{K}_{32}\mathcal{K}_{45}\mathcal{K}_{54} + \mathcal{K}_{22}\mathcal{K}_{33}\mathcal{K}_{44}\mathcal{K}_{56}\mathcal{K}_{65} \\ &- \mathcal{K}_{44}\mathcal{K}_{23}\mathcal{K}_{32}\mathcal{K}_{56}\mathcal{K}_{65} + \mathcal{K}_{22}\mathcal{K}_{34}\mathcal{K}_{43}\mathcal{K}_{56}\mathcal{K}_{65})\end{aligned} \tag{19}$$

Additionally, the material overlay in the vertices can be removed with the aid of the method of mass multiple counting proposed by Hedayati et al. [74], so the mass density of the nanoporous biomaterial including truncated cube cells can be evaluated as a function of pore size (ℓ/r) as below

$$\rho=V^*\bar{\rho}=\frac{24\left(\frac{\pi}{2}\frac{\ell}{r}-2.5758\right)+12\left(\frac{\pi}{4}\frac{\ell}{r}-1.2879\right)}{\left(1+\sqrt{2}\right)^3\left(\frac{\ell}{r}\right)^3}\bar{\rho} \tag{20}$$

where $\bar{\rho}$ is the mass density of the material without porosity, and V^* is the occupied volume of the complete cube to the occupied volume of the truncated cube ratio.

This point should be noted that in the current study, it is assumed that ℓ/r represents the influence of the porosity on the ratio of the volume occupied by the material to the total volume of the unit cell, so it is named as pore size.

3. Size-dependent modeling of a micro/nano-beam made of nanoporous biomaterial

The components of the displacement vector along different coordinate directions for a beam-type structure as shown in Figure 1 take the following forms

$$u_x(x,t) = u(x,t) - z\frac{\partial w(x,t)}{\partial x} \tag{21a}$$

$$u_z(x,t) = w(x,t) \tag{21b}$$

in which u and w stand for the scalar displacement parameters of the micro/nano-beam along *x*- and *z*-axis, respectively.

Accordingly, the non-zero nonlinear strain component can be given as

$$\varepsilon_{xx} = \frac{\partial u}{\partial x} - z\frac{\partial^2 w}{\partial x^2} + \frac{1}{2}\left(\frac{\partial w}{\partial x}\right)^2 \tag{22}$$

In order to incorporate simultaneously the both hardening-stiffness and softening-stiffness influences of size dependency at nanoscale, Lim et al. [52] proposed a new size-dependent continuum theory of elasticity namely as nonlocal strain gradient elasticity theory. In accordance with this theory, the strain energy of a nanostructure can be evaluated as

$$\Pi_s = \frac{1}{2}\int_V \{\sigma_{ij}\varepsilon_{ij} + \sigma_{ij}^*\varepsilon_{ij,k}\}dV \tag{23}$$

where σ_{ij} and σ_{ij}^* are, respectively, the nonlocal and higher-order nonlocal stress tensors which can be introduced as

$$\sigma_{ij} = \int_V \{\varrho_1(|\mathcal{X}' - \mathcal{X}|, \mu)C_{ijkl}\varepsilon_{ij}\}dV \tag{24a}$$

$$\sigma_{ij}^* = l^2\int_V \{\varrho_2(|\mathcal{X}' - \mathcal{X}|, \mu)C_{ijkl}\varepsilon_{ij,k}\}dV \tag{24b}$$

in which l denotes the strain gradient parameter to consider the deformation at microscale, ϱ_1 and ϱ_2 are the attenuation nonlocal kernel functions associated with the classical and strain gradient stress tensors, respectively. Also, C is the elastic matrix, $\mathcal{X}$ and $\mathcal{X}'$ in order represent a point and any point else in the body, μ stands for the nonlocal parameter.

Following the method of Eringen, the non-classical stress-strain relationships become

$$(1 - \mu^2\nabla^2)\sigma_{ij} = C_{ijkl}\varepsilon_{kl} \tag{25a}$$

$$(1 - \mu^2\nabla^2)\sigma_{ij}^* = l^2C_{ijkl}\varepsilon_{kl,m} \tag{25b}$$

In which μ is the nonlocal parameter.

On the other hand, based upon the nonlocal strain gradient theory of elasticity, the constitutive relationship corresponding to the total nonlocal strain gradient stress tensor can be expressed as

$$\mathcal{T}_{ij} = \sigma_{ij} - \nabla\sigma_{ij}^{*} \tag{26}$$

As a result, the general nonlocal strain gradient constitutive equation can be written as

$$(1-\mu^2\nabla^2)\mathcal{T}_{ij} = C_{ijkl}(1-l^2\nabla^2)\varepsilon_{kl} \tag{27}$$

For a beam-type structure, one will have

$$\left(1-\mu^2\frac{\partial^2}{\partial x^2}\right)\mathcal{T}_{xx} = \left(\frac{E}{1-\nu^2}\right)\left(\frac{\partial u}{\partial x} - z\frac{\partial^2 w}{\partial x^2} + \frac{1}{2}\left(\frac{\partial w}{\partial x}\right)^2\right) - \left(\frac{E}{1-\nu^2}\right)l^2\frac{\partial^2}{\partial x^2}\left(\frac{\partial u}{\partial x} - z\frac{\partial^2 w}{\partial x^2} + \frac{1}{2}\left(\frac{\partial w}{\partial x}\right)^2\right) \tag{28}$$

Thus the strain energy associated with a micro/nano-beam on the basis of the nonlocal strain gradient elasticity theory can be obtained as

$$\Pi_s = \frac{1}{2}\int_0^L \left\{N_{xx}\left(\frac{\partial u}{\partial x} + \frac{1}{2}\left(\frac{\partial w}{\partial x}\right)^2\right) - M_{xx}\frac{\partial^2 w}{\partial x^2}\right\}dx \tag{29}$$

where the stress resultants are in the following forms

$$N_{xx} - \mu^2\frac{\partial^2 N_{xx}}{\partial x^2} = A_{11}\left(1-l^2\frac{\partial^2}{\partial x^2}\right)\left(\frac{\partial u}{\partial x} + \frac{1}{2}\left(\frac{\partial w}{\partial x}\right)^2\right) \tag{30a}$$

$$M_{xx} - \mu^2\frac{\partial^2 M_{xx}}{\partial x^2} = -D_{11}\left(1-l^2\frac{\partial^2}{\partial x^2}\right)\frac{\partial^2 w}{\partial x^2} \tag{30b}$$

where

$$\{N_{xx}, M_{xx}\} = b\int_{-\frac{h}{2}}^{\frac{h}{2}} \mathcal{T}_{xx}\{1, z\}dz \tag{31}$$

$$\{A_{11}, D_{11}\} = \frac{Eb}{1-\nu^2}\int_{-\frac{h}{2}}^{\frac{h}{2}}\{1, z^2\}dz = \left\{\frac{Ebh}{1-\nu^2}, \frac{Ebh^3}{12(1-\nu^2)}\right\}$$

Moreover, the kinematic energy of the micro/nano-beam can be defined as

$$\Pi_T = \frac{1}{2}\int_V \rho\left\{\left(\frac{\partial u_x}{\partial t}\right)^2 + \left(\frac{\partial u_z}{\partial t}\right)^2\right\}dV = \frac{1}{2}\int_x \left\{\rho bh\left(\frac{\partial u}{\partial t}\right)^2 + \rho bh\left(\frac{\partial w}{\partial t}\right)^2 + \frac{\rho bh^3}{12}\left(\frac{\partial^2 w}{\partial x\partial t}\right)^2\right\}dx \tag{32}$$

Additionally, the work done by the external distributed load f can be given as

$$\Pi_P = \int_x f(x,t)w\,dx \tag{33}$$

By using the Hamilton's principle, one obtains the following differential equations

$$\frac{\partial N_{xx}}{\partial x} = I_1 \frac{\partial^2 u}{\partial t^2} \tag{34a}$$

$$\frac{\partial}{\partial x}\left[N_{xx}\frac{\partial w}{\partial x}\right] + \frac{\partial^2 M_{xx}}{\partial x^2} = f + I_1\frac{\partial^2 w}{\partial t^2} - I_3\frac{\partial^4 w}{\partial x^2 \partial t^2} \tag{34b}$$

in which

$$\{I_1, I_3\} = b\int_{-\frac{h}{2}}^{\frac{h}{2}} \rho\{1, z^2\}dz = \left\{\rho bh, \frac{\rho bh^3}{12}\right\} \tag{35}$$

In the fast dynamic problem, it can be assumed that $\frac{\partial^2 u}{\partial t^2} = 0$. Therefore, based on equation (34a), one will have $N_{xx} = c$, where c is a constant. In addition, for immovable end supports, it yields

$$N_{xx} = \frac{A_{11}}{2L}\int_0^L \left(\frac{\partial w}{\partial x}\right)^2 dx \tag{36}$$

Consequently, equation (34b) can be expressed in terms of the displacement field as below

$$-D_{11}\left(1 - l^2\frac{\partial^2}{\partial x^2}\right)\frac{\partial^4 w}{\partial x^4} + \left[\frac{A_{11}}{2L}\int_0^L \left(\frac{\partial w}{\partial x}\right)^2 dx\right]\left(1 - \mu^2\frac{\partial^2}{\partial x^2}\right)\frac{\partial^2 w}{\partial x^2} = \left(1 - \mu^2\frac{\partial^2}{\partial x^2}\right)\left(f + I_1\frac{\partial^2 w}{\partial t^2} - I_3\frac{\partial^4 w}{\partial x^2 \partial t^2}\right) \tag{37}$$

This point should be mentioned here that the nonlocal stress and strain gradient size dependencies are taken into account via the unconventional continuum theories applied to the stress-strain constitutive equations of the micro/nano-structure. As a result, the material properties are the same based on the both classical (local) and nonlocal strain gradient elasticity theories, and they are independent of the size effects. Therefore, in the analytical solution for capturing the material properties of the porous material properties, the classical (local) elasticity is put to use. But for the vibrational resonance analysis of the micro/nano-beam made of this porous material, the size effects are considered based upon the nonlocal strain gradient theory of elasticity.

4. Multiple time-scales solving process

In order to perform the solving process in a more general form, the following dimensionless parameters are taken into account

$$W = \frac{w}{h}, \quad X = \frac{x}{L}, \quad \vartheta = \frac{h}{L}, \quad T = \frac{t}{L}\sqrt{\frac{E_0}{\rho_0}}, \quad \{\hat{I}_1, \hat{I}_3\} = \left\{\frac{I_1}{\rho_0 bh}, \frac{I_3}{\rho_0 bh^3}\right\}$$
$$F = \frac{fL^2}{E_0 bh^2}, \quad a_{11} = \frac{A_{11}}{E_0 bh}, \quad d_{11} = \frac{D_{11}}{E_0 bh^3}, \quad \mathcal{G}_1 = \frac{l}{L}, \quad \mathcal{G}_2 = \frac{\mu}{L} \tag{38}$$

where E_0 and ρ_0 are the young's modulus and mass density of the nanoporous biomaterial with pore size of $\ell / r = 10$.

Therefore, the dimensionless form of the size-dependent nonlinear governing differential equation of motion takes the following form

$$-d_{11}\vartheta^2\left(1-\mathcal{G}_1^2\frac{\partial^2}{\partial X^2}\right)\frac{\partial^4 W}{\partial X^4}+\left[\frac{a_{11}\vartheta^2}{2}\int_0^1\left(\frac{\partial W}{\partial X}\right)^2 dX\right]\left(1-\mathcal{G}_2^2\frac{\partial^2}{\partial X^2}\right)\frac{\partial^2 W}{\partial X^2}$$
$$=\left(1-\mathcal{G}_2^2\frac{\partial^2}{\partial X^2}\right)\left(F+\hat{I}_1\frac{\partial^2 W}{\partial T^2}-\hat{I}_3\vartheta^2\frac{\partial^4 W}{\partial X^2\partial T^2}\right) \tag{39}$$

With the aid of the Galerkin technique, the governing differential equation can be written in discretized form. To this end, it is assumed that $W(X,T)$ can be expressed separately as below

$$W(X,T)=\varphi(X)q(T) \tag{40}$$

By inserting equation (40) in equation (39), one obtains

$$-d_{11}\vartheta^2 q\left(\frac{d^4\varphi}{dX^4}-\mathcal{G}_1^2\frac{d^6\varphi}{dX^6}\right)+\frac{a_{11}\vartheta^2 q^3}{2}\left[\int_0^1\left(\frac{d\varphi}{dX}\right)^2 dX\right]\left(\frac{d^2\varphi}{dX^2}-\mathcal{G}_2^2\frac{d^4\varphi}{dX^4}\right)$$
$$=F-\mathcal{G}_2^2\frac{\partial^2 F}{\partial X^2}+\hat{I}_1\left(\varphi\frac{d^2 q}{dT^2}-\mathcal{G}_2^2\frac{d^2\varphi}{dX^2}\frac{d^2 q}{dT^2}\right)-\hat{I}_3\vartheta^2\left(\frac{d^2\varphi}{dX^2}\frac{dq^2}{dT^2}-\mathcal{G}_2^2\frac{d^4\varphi}{dX^4}\frac{d^2 q}{dT^2}\right) \tag{41}$$

By employing the Galerkin technique, the Duffing type equation of motion can be extracted in the following form

$$\ddot{q}+2\beta\dot{q}+\omega^2 q+\alpha q^3=\tilde{F} \tag{42}$$

in which

$$\omega^2=-\frac{\int_0^1\left\{-d_{11}\vartheta^2\varphi\left(\frac{d^4\varphi}{dX^4}-\mathcal{G}_1^2\frac{d^6\varphi}{dX^6}\right)\right\}dX}{\int_0^1\left\{\hat{I}_1\varphi\left(\varphi-\mathcal{G}_2^2\frac{d^2\varphi}{dX^2}\right)-\hat{I}_3\vartheta^2\varphi\left(\frac{d^2\varphi}{dX^2}-\mathcal{G}_2^2\frac{d^4\varphi}{dX^4}\right)\right\}dX}$$

$$\alpha=-\frac{\int_0^1\left\{\frac{a_{11}\vartheta^2\varphi}{2}\left[\int_0^1\left(\frac{d\varphi}{dX}\right)^2 dX\right]\left(\frac{d^2\varphi}{dX^2}-\mathcal{G}_2^2\frac{d^4\varphi}{dX^4}\right)\right\}dX}{\int_0^1\left\{\hat{I}_1\varphi\left(\varphi-\mathcal{G}_2^2\frac{d^2\varphi}{dX^2}\right)-\hat{I}_3\vartheta^2\varphi\left(\frac{d^2\varphi}{dX^2}-\mathcal{G}_2^2\frac{d^4\varphi}{dX^4}\right)\right\}dX} \tag{43}$$

$$\tilde{F}=-\frac{F-\mathcal{G}_2^2\frac{\partial^2 F}{\partial X^2}}{\int_0^1\left\{\hat{I}_1\varphi\left(\varphi-\mathcal{G}_2^2\frac{d^2\varphi}{dX^2}\right)-\hat{I}_3\vartheta^2\varphi\left(\frac{d^2\varphi}{dX^2}-\mathcal{G}_2^2\frac{d^4\varphi}{dX^4}\right)\right\}dX}$$

Also, it is assumed that the external distributed load is a dissipative one, so the damping parameter takes the following form

$$\beta=\frac{\eta\omega^2}{\omega_L} \tag{44}$$

where ω_L represents the linear frequency of the system and η is a constant.

The analytical expression for $\varphi(X)$ corresponding to each type of boundary conditions can be introduced as [75]

- For simply supported-simply supported boundary conditions:

$$\varphi(X) = \sin(\pi X) \tag{45}$$

- For clamped-clamped boundary conditions:

$$\varphi(X) = \cos(4.73X) - \cosh(4.73X) + \left(\frac{\cos(4.73) - \cosh(4.73)}{\sin(4.73) - \sinh(4.73)}\right)(\sinh(4.73X) - \sin(4.73X)) \tag{46}$$

- For simply supported-clamped boundary conditions:

$$\varphi(X) = \cos(3.927X) - \cosh(3.927X) + \left(\frac{\cos(3.927) - \cosh(3.927)}{\sin(3.927) - \sinh(3.927)}\right)(\sinh(3.927X) - \sin(3.927X)) \tag{47}$$

The damping and nonlinear terms are supposed to be small and they are in order of a small parameter, ϵ. Consequently, equation (42) takes the following form

$$\ddot{q} + 2\beta\epsilon\dot{q} + \omega^2 q + \alpha\epsilon q^3 = \tilde{F} \tag{48}$$

For the hard excitation, the order of the external distributed load is higher than that of damping and nonlinear terms. Therefore, for a periodic type of excitation, one will have

$$\ddot{q}(T) + 2\beta\epsilon\dot{q}(T) + \omega^2 q(T) + \alpha\epsilon q^3(T) = 2\tilde{F}\cos(\varOmega T) \tag{49}$$

where $\varOmega$ is the excitation frequency.

On the other hand, the following multiple time-scales summation is considered for q:

$$q(T) = q_0(T_0, T_1) + \epsilon q_1(T_0, T_1) \tag{50}$$

in which $T_0 = T$ and $T_1 = \epsilon T$. By inserting equation (50) in equation (49), it yields

$$\begin{cases} O(\epsilon^0): \mathcal{D}_0^2 q_0 + \omega^2 q_0 = 2\tilde{F}\cos(\varOmega T_0) \\ O(\epsilon^1): \mathcal{D}_0^2 q_1 + \omega^2 q_1 = -2\mathcal{D}_0\mathcal{D}_1 q_0 - 2\beta\mathcal{D}_0 q_0 - \alpha q_0^3 \end{cases} \tag{51}$$

where $\mathcal{D}_i^j = \frac{d^j}{dT_i^j}$ are time derivatives.

Based upon the first relation of equation (51), one will have

$$q_0 = \mathcal{A}(T_1)e^{i\omega T_0} + \Delta e^{i\omega T_0} + \mathcal{B}(T_1)e^{i\omega T_0} \tag{52}$$

in which $\mathcal{B}(T_1)$ stands for the complex conjugate part of the expression, and

$$\Delta = \frac{\tilde{F}}{\omega^2 - \varOmega^2} \tag{53}$$

Afterwards, substitution of equation (52) in the second relation of equation (51) yields

$$\begin{aligned} \mathcal{D}_0^2 q_1 + \omega^2 q_1 = &-\left[2i\omega_0\left(\frac{d\mathcal{A}}{dT_1} + \mathcal{A}\beta\right) + 6\alpha\mathcal{A}\Delta^2 + 3\alpha\mathcal{A}^2\mathcal{B}\right]e^{i\omega T_0} \\ &- \alpha\left\{\mathcal{A}^3 e^{3i\omega T_0} + \Delta^3 e^{3i\omega T_0} + 3\mathcal{A}^2\Delta e^{i(2\omega+\varOmega)T_0} + 3\Delta\left(\frac{d\mathcal{A}}{dT_1}\right)^2 e^{i(\varOmega-2\omega)T_0}\right. \\ &\left. + 3\mathcal{A}\Delta^2 e^{i(\omega+2\varOmega)T_0} + 3\mathcal{A}\Delta^2 e^{i(\omega-2\varOmega)T_0} - \Delta\left[2i\beta\varOmega + 3\alpha\Delta^2 + 6\alpha\mathcal{A}\left(\frac{d\mathcal{A}}{dT_1}\right)\right]e^{i\omega T_0}\right\} \\ &+ \cdots \end{aligned} \tag{54}$$

4.1. Superharmonic excitation

Within the range of superharmonic excitation, it can be written

$$3\Omega = \omega + \epsilon\Gamma \tag{55}$$

where Γ represents the detuning parameter. By setting the secular and small divisor terms equal to zero, one will have

$$2i\omega_0\left(\frac{d\mathcal{A}}{dT_1} + \mathcal{A}\beta\right) + 6\alpha\mathcal{A}\Delta^2 + 3\alpha\mathcal{A}^2\mathcal{B} + \alpha\Delta^3 e^{3i\Gamma T_1} = 0 \tag{56}$$

For $\mathcal{A}(T_1)$, A polar function is considered as below

$$\mathcal{A}(T_1) = \frac{1}{2}a(T_1)e^{i\xi(T_1)} \tag{57}$$

Through substitution of equation (57) into equation (56), each of the real and imaginary parts gives

$$\frac{da}{dT_1} = -\beta a + \frac{1}{2}\frac{\alpha\Delta^3}{\omega}\sin(\Gamma T_1 - \xi) \tag{58a}$$

$$a\frac{d\xi}{dT_1} = \frac{3\alpha a}{\omega}\left(\Delta^2 + \frac{a^2}{8}\right) + \frac{\alpha\Delta^3}{\omega}\cos(\Gamma T_1 - \xi) \tag{58b}$$

By setting the derivative terms on the left side of equation (58) equal to zero, the steady-state solution can be captured as

$$\left[\beta^2 + \left(\Gamma - \frac{3\alpha\Delta^2}{\omega} - \frac{3\alpha a^2}{8\omega}\right)^2\right]a^2 = \frac{\alpha^2\Delta^6}{\omega^2} \tag{59}$$

Therefore, the size-dependent frequency-response associated with the superharmonic excitation of a micro/nano-beam can be given as

$$\Gamma = \frac{3\alpha\Delta^2}{\omega} + \frac{3\alpha a^2}{8\omega} \pm \sqrt{\frac{\alpha^2\Delta^6}{a^2\omega^2} - \beta^2} \tag{60}$$

Equation (39) can be rewritten as

$$\left(\beta^2 + \Gamma^2 + \frac{9\alpha^2\Delta^4}{\omega^2} + \frac{9\alpha^2 a^4}{64\omega^2} - \frac{6\alpha\Delta^2\Gamma}{\omega} - \frac{3\alpha a^2\Gamma}{4\omega} + \frac{9\alpha^2 a^2\Delta^2}{4\omega^2}\right)a^2 = \frac{\alpha^2\Delta^6}{\omega^2} \tag{61}$$

As a consequent, one will have

$$\varsigma_1\Delta^6 + \varsigma_2\Delta^4 + \varsigma_3\Delta^2 + \varsigma_4 = 0 \tag{62}$$

in which

$$\varsigma_1 = \frac{\alpha^2}{\omega^2} \quad , \quad \varsigma_2 = -\frac{9\alpha^2 a^2}{\omega^2} \quad , \quad \varsigma_3 = \frac{6\alpha\Gamma a^2}{\omega} - \frac{9\alpha^2 a^4}{4\omega^2}$$

$$\varsigma_4 = -\left(\beta^2 + \Gamma^2 + \frac{9\alpha^2 a^4}{64\omega^2} - \frac{3\alpha a^2 \Gamma}{4\omega}\right) a^2 \tag{63}$$

The solution of equation (62) represents the size-dependent amplitude-response related to the superharmonic excitation of a micro/nano-beam.

4.2. Subharmonic excitation

Within the range of subharmonic excitation, it can be written

$$\Omega = 3\omega + \epsilon\Gamma \tag{64}$$

After that, in accordance with equation (54), the secular and small divisor terms are set equal to zero as below

$$2i\omega_0\left(\frac{d\mathcal{A}}{dT_1} + \mathcal{A}\beta\right) + 6\alpha\mathcal{A}\Delta^2 + 3\alpha\mathcal{A}^2\mathcal{B} + 3\Delta\left(\frac{d\mathcal{A}}{dT_1}\right)^2 e^{i\Gamma T_1} = 0 \tag{65}$$

By equation (57), a polar function is introduced for $\mathcal{A}(T_1)$, so one will have

$$\frac{da}{dT_1} = -\beta a - \frac{3}{4}\frac{\alpha a^2\Delta}{\omega}\sin(\Gamma T_1 - 3\xi) \tag{66a}$$

$$a\frac{d\xi}{dT_1} = \frac{3\alpha a}{\omega}\left(\Delta^2 + \frac{a^2}{8}\right) + \frac{3}{4}\frac{\alpha a^2\Delta}{\omega}\cos(\Gamma T_1 - 3\xi) \tag{66b}$$

To capture the steady-state solution, the derivative terms on the left side of equation (66) are set to be zero. As a result, it yields

$$9\beta^2 + \left(\Gamma - \frac{9\alpha\Delta^2}{\omega} - \frac{9\alpha a^2}{8\omega}\right)^2 = \frac{81\alpha^2 a^2\Delta^2}{16\omega^2} \tag{67}$$

Thus the size-dependent frequency-response associated with the subharmonic excitation of a micro/nano-beam can be presented as

$$\Gamma = \frac{9\alpha\Delta^2}{\omega} + \frac{9\alpha a^2}{8\omega} \pm \sqrt{\frac{81\alpha^2 a^2\Delta^2}{16\omega^2} - 9\beta^2} \tag{68}$$

Additionally, equation (67) can be rewritten as

$$\left(9\beta^2 + \Gamma^2 + \frac{81\alpha^2\Delta^4}{\omega^2} + \frac{81\alpha^2 a^4}{64\omega^2} - \frac{18\alpha\Delta^2\Gamma}{\omega} - \frac{9\alpha a^2\Gamma}{4\omega} + \frac{81\alpha^2 a^2\Delta^2}{4\omega^2}\right) = \frac{81\alpha^2 a^2\Delta^2}{16\omega^2} \tag{69}$$

So, one obtains

$$\mathcal{S}_1\Delta^4 + \mathcal{S}_2\Delta^2 + \mathcal{S}_3 = 0 \tag{70}$$

where

$$\mathcal{S}_1 = \frac{81\alpha^2}{\omega^2} \quad , \quad \mathcal{S}_2 = \frac{243\alpha^2 a^2}{16\omega^2} - \frac{18\alpha\Gamma}{\omega}$$

$$\mathcal{S}_3 = 9\beta^2 + \Gamma^2 + \frac{81\alpha^2 a^4}{64\omega^2} - \frac{9\alpha a^2 \Gamma}{4\omega} \tag{71}$$

The solution of equation (70) yields the size-dependent amplitude-response associated with the subharmonic excitation of a micro/nano-beam.

5. Numerical results and discussion

Now, based upon the captured mechanical properties of the nanoporous biomaterials as functions of pore size, the nonlinear secondary resonance of a micro/nano-beam made of this material under subharmonic and superharmonic excitations is numerically depicted corresponding to different pore sizes. For the micro/nano-beam, it is assumed that $b = h = 2\ nm, L/h = 20, \tilde{F} = 0.1$, and $\eta = 0.5$.

Figures 4 and 5 illustrate, respectively, the nonlocal size effect on the frequency-response of a micro/nano-beam with pore size of $\ell/r = 10$ under the superharmonic and subharmonic excitations. It is revealed that in the case of superharmonic excitation, the jump phenomenon occurs and the nonlocality causes to enhance the both of nonlinear hardening spring-type behavior and the height of limit point bifurcations. In the case of subharmonic excitation, there is two branches including the high-frequency and low-frequency solutions. By taking the nonlocality into consideration, the gap between these branches increases.

In Figures 6 and 7, the strain gradient size dependency in the frequency-response of a micro/nano-beam with pore size of $\ell/r = 10$ is shown corresponding to the superharmonic and subharmonic excitations, respectively. It can be seen that in the case of superharmonic excitation, the strain gradient size effect leads to reduce the nonlinear hardening spring-type behavior as well as the height of limit point bifurcations. For subharmonic case of study, the strain gradient size dependency causes to decrease the gap between two branches associated with the high-frequency and low-frequency solutions.

The influence of nonlocality on the amplitude-response of a micro/nano-beam with pore size of $\ell/r = 10$ is depicted in Figures 8 and 9 corresponding to, respectively, the superharmonic and subharmonic excitations. It is observed that in the superharmonic case, the both types of upward jump and downward jump exist. By taking nonlocal size effect, the maximum amplitude of the response related to downward jump decreases, so through reduction of the amplitude of the excitation, the amplitude of the responses vanishes less rapidly. For the subharmonic case, it is indicated that the micro/nano-beam is excited within a specific range of the amplitude of the excitation. The wide of this range becomes lower by taking the nonlocal size effect into account.

Figures 10 and 11 display, respectively, the strain gradient size effect on the amplitude-response of a micro/nano-beam with pore size of $\ell/r = 10$ subjected to the superharmonic and subharmonic excitations. It is found that for superharmonic excitation, the strain gradient size dependency leads to increase the maximum amplitude of the response related to downward jump. As a result, by decreasing the amplitude of the excitation, the amplitude of the responses vanishes more rapidly. Also, in the case of subharmonic excitation, the range of amplitude of the excitation within which, the micro/nano-beam is excited becomes wider due to the strain gradient size effect.

In order to compare the significance of the two different size dependencies, in Table 1, the influences of the nonlocality and strain gradient size dependency on the natural frequency of a micro/nano-beam made of nanoporous biomaterial with pore size of $\ell/r = 10$ are represented corresponding to different boundary conditions. The percentages given in the parentheses indicate the difference of the size-dependent natural frequency with its classical counterpart. It can be found that the both nonlocality and strain gradient size dependency have the minimum and maximum influences on the natural frequency of the micro/nano-beam with clamped and simply supported edge supports, respectively. Moreover, by increasing the values of small scale parameters, the influence of the strain gradient size effect is more than that of the nonlocal one.

In Figures 12 and 13, the frequency-response of a micro/nano-beam made of the nanoporous biomaterial with various pores sizes is demonstrated corresponding to the superharmonic and subharmonic excitations, respectively. It can be observed that in the superharmonic case, increasing the pore size leads to enhance the nonlinear hardening spring-type behavior and the height of limit point bifurcations. In the subharmonic case, higher pore size causes to increase the gap between two branches related to the high-frequency and low-frequency solutions.

The influence of pore size on the amplitude-response of a micro/nano-beam made of the nanoporous biomaterial is plotted in Figures 14 and 15 for the superharmonic and subharmonic excitations, respectively. In the superharmonic case, it can be found that by increasing the pore size, the maximum amplitude of the response related to downward jump enhances, so reduction in the amplitude of the excitation leads to vanish the amplitude of the responses more rapidly. In the subharmonic case, it is revealed that increasing the pore size causes to make wider the range of amplitude of the excitation within which, the micro/nano-beam is excited.

6. Concluding remarks

The objective of the current study was to analyze the size-dependent nonlinear secondary resonance of a micro/nano-beam made of nanoporous biomaterials. On the basis of a refined truncated cubic unit cell, analytical expressions for the mechanical properties of the nanoporous biomaterial were obtained as functions of pore size. Subsequently, the Galerkin technique together with the multiple time-scales method was employed to predict the size-dependent frequency-response and amplitude-response of the micro/nano-beam with different pore sizes and end supports corresponding to the subharmonic and superharmonic excitations.

It was demonstrated that in the case of superharmonic excitation, the jump phenomenon occurs and the nonlocality and strain gradient size dependencies cause, respectively, to increase and decrease the both of nonlinear hardening spring-type behavior and the height of limit point bifurcations. In the case of subharmonic excitation, there is two branches including the high-frequency and low-frequency solutions. By taking the nonlocal and strain gradient size effects into consideration, the gap between these branches increases and decreases, respectively. Additionally, it was seen that the both nonlocality and strain gradient size dependency have the minimum and maximum influences on the natural frequency of the micro/nano-beam with clamped and simply supported edge supports, respectively. Furthermore, it was observed that in the superharmonic case, by increasing the pore size, the maximum amplitude of the response related to downward jump enhances, so reduction in the amplitude of the excitation leads to vanish the amplitude of the responses more rapidly. In the subharmonic case, it was found that increasing the pore size causes to make wider the range of amplitude of the excitation within which, the micro/nano-beam is excited.

Appendix A

$$\mathcal{K}_{11} = \frac{2\bar{A}\bar{E}}{\ell} \quad , \quad \mathcal{K}_{21} = -\frac{2\bar{A}\bar{E}}{\ell} \quad , \quad \mathcal{K}_{31} = \mathcal{K}_{41} = \mathcal{K}_{51} = \mathcal{K}_{61} = 0$$

$$\mathcal{K}_{12} = -\frac{2\bar{A}\bar{E}}{\ell} \quad , \quad \mathcal{K}_{42} = \mathcal{K}_{62} = 0$$

$$\mathcal{K}_{22} = \frac{4\bar{A}\bar{E}}{\ell} + \frac{1}{\frac{\ell^3}{24\bar{E}\bar{I}} + \frac{3\ell}{10\bar{G}\bar{A}} + \frac{3}{5\bar{G}\bar{A}}\left(\frac{\left(1+\frac{\wp\ell}{2}\right)\cosh(\wp\ell) - \left(1+\frac{\wp\ell}{2}\right)\sinh(\wp\ell) - 1}{\wp}\right)}$$

$$\mathcal{K}_{32} = -\frac{2\bar{A}\bar{E}}{\ell} - \frac{1}{\frac{\ell^3}{24\bar{E}\bar{I}} + \frac{3\ell}{10\bar{G}\bar{A}} + \frac{3}{5\bar{G}\bar{A}}\left(\frac{\left(1+\frac{\wp\ell}{2}\right)\cosh(\wp\ell) - \left(1+\frac{\wp\ell}{2}\right)\sinh(\wp\ell) - 1}{\wp}\right)}$$

$$\mathcal{K}_{52} = -\frac{2\bar{A}\bar{E}}{\ell} + \frac{1}{\frac{\ell^3}{24\bar{E}\bar{I}} + \frac{3\ell}{10\bar{G}\bar{A}} + \frac{3}{5\bar{G}\bar{A}}\left(\frac{\left(1+\frac{\wp\ell}{2}\right)\cosh(\wp\ell) - \left(1+\frac{\wp\ell}{2}\right)\sinh(\wp\ell) - 1}{\wp}\right)}$$

$$\mathcal{K}_{13} = \mathcal{K}_{53} = \mathcal{K}_{63} = 0$$

$$\mathcal{K}_{23} = \mathcal{K}_{43} = \frac{2\bar{A}\bar{E}}{\ell} - \frac{1}{\frac{\ell^3}{24\bar{E}\bar{I}} + \frac{3\ell}{10\bar{G}\bar{A}} + \frac{3}{5\bar{G}\bar{A}}\left(\frac{\left(1 + \frac{p\ell}{2}\right)\cosh(p\ell) - \left(1 + \frac{p\ell}{2}\right)\sinh(p\ell) - 1}{p}\right)}$$

$$\mathcal{K}_{33} = \frac{4\bar{A}\bar{E}}{\ell} + \frac{1}{\frac{\ell^3}{48\bar{E}\bar{I}} + \frac{3\ell}{20\bar{G}\bar{A}} + \frac{3}{10\bar{G}\bar{A}}\left(\frac{\left(1 + \frac{p\ell}{2}\right)\cosh(p\ell) - \left(1 + \frac{p\ell}{2}\right)\sinh(p\ell) - 1}{p}\right)}$$

$$\mathcal{K}_{14} = \mathcal{K}_{24} = \mathcal{K}_{64} = 0$$

$$\mathcal{K}_{34} = -\frac{2\bar{A}\bar{E}}{\ell} - \frac{1}{\frac{\ell^3}{24\bar{E}\bar{I}} + \frac{3\ell}{10\bar{G}\bar{A}} + \frac{3}{5\bar{G}\bar{A}}\left(\frac{\left(1 + \frac{p\ell}{2}\right)\cosh(p\ell) - \left(1 + \frac{p\ell}{2}\right)\sinh(p\ell) - 1}{p}\right)}$$

$$\mathcal{K}_{44} = \frac{4\bar{A}\bar{E}}{\ell} + \frac{1}{\frac{\ell^3}{24\bar{E}\bar{I}} + \frac{3\ell}{10\bar{G}\bar{A}} + \frac{3}{5\bar{G}\bar{A}}\left(\frac{\left(1 + \frac{p\ell}{2}\right)\cosh(p\ell) - \left(1 + \frac{p\ell}{2}\right)\sinh(p\ell) - 1}{p}\right)}$$

$$\mathcal{K}_{54} = \frac{4\bar{A}\bar{E}}{\ell} + \frac{1}{\frac{\ell^3}{24\bar{E}\bar{I}} + \frac{3\ell}{10\bar{G}\bar{A}} + \frac{3}{5\bar{G}\bar{A}}\left(\frac{\left(1 + \frac{p\ell}{2}\right)\cosh(p\ell) - \left(1 + \frac{p\ell}{2}\right)\sinh(p\ell) - 1}{p}\right)}$$

$$\mathcal{K}_{15} = \mathcal{K}_{35} = 0$$

$$\mathcal{K}_{25} = -\frac{2\bar{A}\bar{E}}{\ell} + \frac{1}{\frac{\ell^3}{24\bar{E}\bar{I}} + \frac{3\ell}{10\bar{G}\bar{A}} + \frac{3}{5\bar{G}\bar{A}}\left(\frac{\left(1 + \frac{p\ell}{2}\right)\cosh(p\ell) - \left(1 + \frac{p\ell}{2}\right)\sinh(p\ell) - 1}{p}\right)}$$

$$\mathcal{K}_{45} = \frac{2\bar{A}\bar{E}}{\ell} - \frac{1}{\frac{\ell^3}{24\bar{E}\bar{I}} + \frac{3\ell}{10\bar{G}\bar{A}} + \frac{3}{5\bar{G}\bar{A}}\left(\frac{\left(1 + \frac{p\ell}{2}\right)\cosh(p\ell) - \left(1 + \frac{p\ell}{2}\right)\sinh(p\ell) - 1}{p}\right)}$$

$$\mathcal{K}_{55} = \frac{20\bar{A}\bar{E}}{\ell} + \frac{1}{\frac{\ell^3}{48\bar{E}\bar{I}} + \frac{3\ell}{20\bar{G}\bar{A}} + \frac{3}{10\bar{G}\bar{A}}\left(\frac{\left(1 + \frac{p\ell}{2}\right)\cosh(p\ell) - \left(1 + \frac{p\ell}{2}\right)\sinh(p\ell) - 1}{p}\right)}$$

$$\mathcal{K}_{65} = -\frac{8\bar{A}\bar{E}}{\ell} \quad , \quad \mathcal{K}_{16} = \mathcal{K}_{26} = \mathcal{K}_{36} = \mathcal{K}_{46} = 0 \quad , \quad \mathcal{K}_{56} = -\frac{8\bar{A}\bar{E}}{\ell} \quad , \quad \mathcal{K}_{66} = \frac{8\bar{A}\bar{E}}{\ell}$$

References

[1] S. Sahmani, M. Shahali, A. Khandan, S. Saber-Samandari, M.M. Aghdam, 2018, Analytical and experimental analyses for mechanical and biological characteristics of novel nanoclay bio-nanocomposite scaffolds fabricated via space holder technique, Applied Clay Science 165, pp. 112-123.

[2] S. Sahmani, S. Saber-Samandari, M. Shahali, H.J. Yekta, F. Aghadavoudi, A.H. Montazeran, M.M. Aghdam, A. Khandan, 2018, Mechanical and biological performance of axially loaded novel bio-nanocomposite sandwich plate-type implant coated by biological polymer thin film, Journal of the Mechanical Behavior of Biomedical Materials 88, pp. 238-250.

[3] S. Sahmani, S. Saber-Samandari, A. Khandan, M.M. Aghdam, 2019, Nonlinear resonance investigation of nanoclay based bio-nanocomposite scaffolds with enhanced properties for bone substitute applications, Journal of Alloys and Compounds 773, pp. 636-653.

[4] J. Safari, Z. Zarnegar, 2014, Advanced drug delivery systems: Nanotechnology of health design A review, Journal of Saudi Chemical Society 18, pp. 85-99.

[5] Y. Usui, J.E. Zerwekh, H. Vanharanta, R.B. Ashman, V. Mooney, 1989, Different effects of mechanical vibration on bone ingrowth into porous hydroxyapatite and fracture healing in a rabbit model, Journal of Orthopaedic Research 7, pp. 559-567.

[6] G. Altintas, 2014, Natural vibration behaviors of heterogeneous porous materials in micro scale, Journal of Vibration and Control 20, pp. 1999-2005.

[7] A.C. Eringen, 1972, Linear theory of nonlocal elasticity and dispersion of plane waves, International Journal of Engineering Science 10, pp. 425-435.

[8] M.E. Gurtin, A.I. Murdoch, 1978, Surface stress in solids, International Journal of Solids and Structures 14, pp. 431-440.

[9] D. Lam, F. Yang, A. Chong, J. Wang, P. Tong, 2003, Experiments and theory in strain gradient elasticity, Journal of Mechanics and Physics in Solids 51, pp. 1477-1508.

[10] F. Yang, A. Chong, D. Lam, P. Tong, 2002, Couple stress based strain gradient theory for elasticity, International Journal of Solids and Structures 39, pp. 2731-2743.

[11] Y.S. Li, Z.Y. Cai, S.Y. Shi, 2014, Buckling and free vibration of magnetoelectroelastic nanoplate based on nonlocal theory, Composite Structures 111, pp. 522-529.

[12] F. Daneshmand, H. Farokhi, M. Amabili, 2014, A higher-order mathematical modeling for dynamic behavior of protein microtubule shell structures including shear deformation and small-scale effects, Mathematical Biosciences 252, pp. 67-82.

[13] M.M.S. Fakhrabadi, A. Rastgoo, M.T. Ahmadian, 2014, Non-linear behaviors of carbon nanotubes under electrostatic actuation based on strain gradient theory, International Journal of Non-Linear Mechanics 67, pp. 236-244.

[14] S. Sahmani, M.M. Aghdam, M. Bahrami, 2015, On the postbuckling behavior of geometrically imperfect cylindrical nanoshells subjected to radial compression including surface stress effects, Composite Structures 131, pp. 414-424.

[15] A. Ghorbanpour Arani, M. Abdollahian, M.H. Jalaei, 2015, Vibration of bioliquid-filled microtubules embedded in cytoplasm including surface effects using modified couple stress theory, Journal of Theoretical Biology 367, pp. 29-38.
[16] J. Zhang, S.A. Meguid, 2016, Effect of surface energy on the dynamic response and instability of fluid-conveying nanobeams, European Journal of Mechanics – A/Solids 58, pp. 1-9.
[17] S. Sahmani, M.M. Aghdam, A.H. Akbarzadeh, 2016, Size-dependent buckling and postbuckling behavior of piezoelectric cylindrical nanoshells subjected to compression and electrical load, Materials & Design 105, pp. 341-351.
[18] M. Shaat, A. Abdelkefi, 2016, Size dependent and micromechanical modeling of strain gradient-based nanoparticle composite plates with surface elasticity, European Journal of Mechanics – A/Solids 58, pp. 54-68.
[19] S. Sahmani, M.M. Aghdam, M. Bahrami, 2017, Surface free energy effects on the postbuckling behavior of cylindrical shear deformable nanoshells under combined axial and radial compressions, Meccanica 52, pp. 1329-1352.
[20] S. Sahmani, M.M. Aghdam, M. Bahrami, 2017, An efficient size-dependent shear deformable shell model and molecular dynamics simulation for axial instability analysis of silicon nanoshells, Journal of Molecular Graphics and Modelling 77, pp. 263-279.
[21] J. Fernandez-Saez, R. Zaera, 2017, Vibrations of Bernoulli-Euler beams using the two-phase nonlocal elasticity theory, International Journal of Engineering Science 119, pp. 232-248.
[22] S. Sahmani, M.M. Aghdam, M. Bahrami, 2017, Nonlinear buckling and postbuckling behavior of cylindrical shear deformable nanoshells subjected to radial compression including surface free energy effects, Acta Mechanica Solida Sinica 30, pp. 209-222.
[23] S. Sahmani, M.M. Aghdam, 2017, Nonlinear vibrations of pre-and post-buckled lipid supramolecular micro/nano-tubules via nonlocal strain gradient elasticity theory, Journal of Biomechanics 65, pp. 49-60.
[24] M. Shaat, A. Abdelkefi, 2017, Material structure and size effects on the nonlinear dynamics of electrostatically-actuated nano-beams, International Journal of Non-Linear Mechanics 89, pp. 25-42.
[25] L.C. Trinh, T.P. Vo, H.-T. Thai, J.L. Mantari, 2017, Size-dependent behaviour of functionally graded sandwich microplates under mechanical and thermal loads, Composites Part B: Engineering 124, pp. 218-241.
[26] S. Sahmani, M.M. Aghdam, 2017, Imperfection sensitivity of the size-dependent postbuckling response of pressurized FGM nanoshells in thermal environments, Archives of Civil and Mechanical Engineering 17, pp. 623-638.
[27] S. Sahmani, A.M. Fattahi, 2017, Imperfection sensitivity of the size-dependent nonlinear instability of axially loaded FGM nanopanels in thermal environments, Acta Mechanica 228, pp. 3789-3810.

[28] K. Mercan, O. Civalek, 2017, Buckling analysis of Silicon carbide nanotubes (SiCNTs) with surface effect and nonlocal elasticity using the method of HDQ, Composites Part B: Engineering 114, pp. 34-45.
[29] S. Sahmani, A.M. Fattahi, 2017, An anisotropic calibrated nonlocal plate model for biaxial instability analysis of 3D metallic carbon nanosheets using molecular dynamics simulations, Materials Research Express 4, pp. 065001.
[30] S. Sahmani, M.M. Aghdam, 2017, Size-dependent nonlinear bending of micro/nano-beams made of nanoporous biomaterials including a refined truncated cube cell, Physics Letters A 381, pp. 3818-3830.
[31] Y. Tadi beni, M. Karimi Zeverdejani, F. Mehralian, 2017, Buckling analysis of orthotropic protein microtubules under axial and radial compression based on couple stress theory, Mathematical Biosciences 292, pp. 18-29.
[32] H.X. Nguyen, E. Atroshchenko, H. Nguyen-Xuan, T.P. Vo, 2017, Geometrically nonlinear isogeometric analysis of functionally graded microplates with the modified couple stress theory, Computers & Structures 193, pp. 110-127.
[33] S. Sahmani, A.M. Fattahi, 2017, Size-dependent nonlinear instability of shear deformable cylindrical nanopanels subjected to axial compression in thermal environments, Microsystem Technologies 23, pp. 4717-4731.
[34] S. Thai, H.-T. Thai, T.P. Vo, H. Nguyen-Xuan, 2017, Nonlinear static and transient isogeometric analysis of functionally graded microplates based on the modified strain gradient theory, Engineering Structures 153, pp. 598-612.
[35] S. Sahmani, M.M. Aghdam, 2017, Axial postbuckling analysis of multilayer functionally graded composite nanoplates reinforced with GPLs based on nonlocal strain gradient theory, The European Physical Journal Plus 132, pp. 490.
[36] J.C. Liu, Y.Q. Zhang, L.F. Fan, 2017, Nonlocal vibration and biaxial buckling of double-viscoelastic-FGM-nanoplate system with viscoelastic Pasternak medium in between, Physics Letters A 381, pp. 1228-1235.
[37] B. Karami, D. Shahsavari, L. Li, 2018, Hygrothermal wave propagation in viscoelastic graphene under in-plane magnetic field based on nonlocal strain gradient theory, Physica E 97, pp. 317-327.
[38] S. Sahmani, A.M. Fattahi, 2018, Small scale effects on buckling and postbuckling behaviors of axially loaded FGM nanoshells based on nonlocal strain gradient elasticity theory, Applied Mathematics and Mechanics 39, pp. 561-580.
[39] Z. Wang, Z. Xie, W. Huang, 2018, A pin-moment model of flexoelectric actuators, International Journal of Hydromechatronics 1, pp. 72-90.
[40] J. Fang, J. Gu, H. Wang, 2018, Size-dependent three-dimensional free vibration of rotating functionally graded microbeams based on a modified couple stress theory, International Journal of Mechanical Sciences 136, pp. 188-199.

[41] S. Sahmani, M.M. Aghdam, 2018, Nonlinear instability of hydrostatic pressurized microtubules surrounded by cytoplasm of a living cell including nonlocality and strain gradient microsize dependency, Acta Mechanica 229, pp. 403-420.
[42] I. Rehab, X. Tian, F. Gu, et al., 2018, The influence of rolling bearing clearances on diagnostic signatures based on a numerical simulation and experimental evaluation, International Journal of Hydromechatronics 1, pp. 16-46.
[43] C.-L. Thanh, P. Phung-Van, C.H. Thai, H. Nguyen-Xuan, A. Wahab, 2018, Isogeometric analysis of functionally graded carbon nanotube reinforced composite nanoplates using modified couple stress theory, Composite Structures 184, pp. 633-649.
[44] S. Sahmani, M.M. Aghdam, 2018, Nonlocal strain gradient shell model for axial buckling and postbuckling analysis of magneto-electro-elastic composite nanoshells, Composites Part B: Engineering 132, pp. 258-274.
[45] S. Sahmani, M.M. Aghdam, 2018, Nonlocal strain gradient beam model for postbuckling and associated vibrational response of lipid supramolecular protein micro/nano-tubules, Mathematical Biosciences 295, pp. 24-35.
[46] J.P. Henderson, A. Plummer, N. Johnston, 2018, An electro-hydrostatic actuator for hybrid active-passive vibration isolation, International Journal of Hydromechatronics 1, pp. 47-71.
[47] L. Chu, G. Dui, C. Ju, 2018, Flexoelectric effect on the bending and vibration responses of functionally graded piezoelectric nanobeams based on general modified strain gradient theory, Composite Structures 186, pp. 39-49.
[48] S. Sahmani, M.M. Aghdam, 2018, Thermo-electro-radial coupling nonlinear instability of piezoelectric shear deformable nanoshells via nonlocal elasticity theory, Microsystem Technologies 24, pp. 1333-1346.
[49] S. Sahmani, A.M. Fattahi, 2018, Small scale effects on buckling and postbuckling behaviors of axially loaded FGM nanoshells based on nonlocal strain gradient elasticity theory, Applied Mathematics and Mechanics 39, pp. 561-580.
[50] K. Zhang, M.-H. Ge, C. Zhao, Z.-C. Deng, X.-J. Xu, 2019, Free vibration of nonlocal Timoshenko beams made of functionally graded materials by Symplectic method, Composites Part B: Engineering 156, pp. 174-184.
[51] A. Sarafraz, S. Sahmani, M.M. Aghdam, 2019, Nonlinear secondary resonance of nanobeams under subharmonic and superharmonic excitations including surface free energy effects, Applied Mathematical Modelling 66, pp. 195-226.
[52] C.W. Lim, G. Zhang, J.N. Reddy, 2015, A higher-order nonlocal elasticity and strain gradient theory and its applications in wave propagation, Journal of Mechanics and Physics of Solids 78, pp. 298-313.
[53] X. Zhu, L. Li, 2017, Twisting statics of functionally graded nanotubes using Eringen's nonlocal integral model, Composite Structures 178, pp. 87-96.

[54] X. Zhu, L. Li, 2017, On longitudinal dynamics of nanorods, International Journal of Engineering Science 120, pp. 129-145.
[55] Y. Tang, Y. Liu, D. Zhao, 2017, Wave dispersion in viscoelastic single walled carbon nanotubes based on the nonlocal strain gradient Timoshenko beam model, Physica E 87, pp. 301-307.
[56] X. Li, L. Li, Y. Hu, Z. Ding, W. Deng, 2017, Bending, buckling and vibration of axially functionally graded beams based on nonlocal strain gradient theory, Composite Structures 165, pp. 250-265.
[57] F. Ebrahimi, A. Dabbagh, 2017, On flexural wave propagation responses of smart FG magneto-electro-elastic nanoplates via nonlocal strain gradient theory, Composite Structures 162, pp. 281-293.
[58] S. Sahmani, M.M. Aghdam, 2017, Size-dependent axial instability of microtubules surrounded by cytoplasm of a living cell based on nonlocal strain gradient elasticity theory, Journal of Theoretical Biology 422, pp. 59-71.
[59] L. Lu, X. Guo, J. Zhao, 2017, Size-dependent vibration analysis of nanobeams based on the nonlocal strain gradient theory, International Journal of Engineering Science 116, pp. 12-24.
[60] S. Sahmani, M.M. Aghdam, 2017, Nonlinear instability of axially loaded functionally graded multilayer graphene platelet-reinforced nanoshells based on nonlocal strain gradient elasticity theory, International Journal of Mechanical Sciences 131-132, pp. 95-106.
[61] X. Zhu, L. Li, 2017, Closed form solution for a nonlocal strain gradient rod in tension, International Journal of Engineering Science 119, pp. 16-28.
[62] S. Sahmani, M.M. Aghdam, 2017, A nonlocal strain gradient hyperbolic shear deformable shell model for radial postbuckling analysis of functionally graded multilayer GPLRC nanoshells, Composite Structures 178, pp. 97-109.
[63] L. Li, Y. Hu, 2017, Post-buckling analysis of functionally graded nanobeams incorporating nonlocal stress and microstructure-dependent strain gradient effects, International Journal of Mechanical Sciences 120, pp. 159-170.
[64] S. Sahmani, M.M. Aghdam, 2017, Nonlocal strain gradient beam model for nonlinear vibration of prebuckled and postbuckled multilayer functionally graded GPLRC nanobeams, Composite Structures 179, pp. 77-88.
[65] S. Sahmani, M.M. Aghdam, 2018, Nonlinear primary resonance of micro/nano-beams made of nanoporous biomaterials incorporating nonlocality and strain gradient size dependency, Results in Physics 8, pp. 879-892.
[66] A.F. Radwan, M. Sobhy, 2018, A nonlocal strain gradient model for dynamic deformation of orthotropic viscoelastic graphene sheets under time harmonic thermal load, Physica B 538, pp. 74-84.
[67] S. Sahmani, M.M. Aghdam, T. Rabczuk, 2018, Nonlinear bending of functionally graded porous micro/nano-beams reinforced with graphene platelets based upon nonlocal strain gradient theory, Composite Structures 186, pp. 68-78.

[68] S. Sahmani, M.M. Aghdam, T. Rabczuk, 2018, A unified nonlocal strain gradient plate model for nonlinear axial instability of functionally graded porous micro/nano-plates reinforced with graphene platelets, Materials Research Express 5, pp. 045048.

[69] S. Sahmani, M.M. Aghdam, T. Rabczuk, 2018, Nonlocal strain gradient plate model for nonlinear large-amplitude vibrations of functionally graded porous micro/nano-plates reinforced with GPLs, Composite Structures 198, pp. 51-62.

[70] L. Li, H. Tang, Y. Hu, 2018, The effect of thickness on the mechanics of nanobeams, International Journal of Engineering Science 123, pp. 81-91.

[71] R. Hedayati, M. Sadighi, M.M. Aghdam, A.A. Zadpoor, 2017, Analytical relationships for the mechanical properties of additively manufactured porous biomaterials based on octahedral unit cells, Applied Mathematical Modelling 46, pp. 408-422.

[72] J. Sun, Y. Yang, D. Wang, 2012, Mechanical properties of Ti-6al-4V octahedral porous material unit formed by selective laser melting, Advances in Mechanical Engineering, Article ID: 427386.

[73] L. Yang, 2015, Experimental-assisted design development for an octahedral cellular structure using additive manufacturing, Rapid Prototyping Journal 21, pp. 168-176.

[74] R. Hedayati, M. Sadighi, M.M. Aghdam, A.A. Zadpoor, 2016, Effect of mass multiple counting on the elastic properties of open-cell regular porous biomaterials, Materials & Design 89, pp. 9-20.

[75] S.S. Rao, 2007, Vibration of continuous systems, Wil

Table 1: Nondimensional natural frequencies ($\boldsymbol{\omega_L}$) of a micro/nano-beam corresponding to various small scale parameters and boundary conditions ($\boldsymbol{\ell/r = 10}$)

Small scale parameters (nm)	C-C boundary conditions	C-SS boundary conditions	SS-SS boundary conditions
$\mu = 0\,, l = 0$	0.6342	0.4531	0.2900
$\mu = 0.5\,, l = 0$	0.6329 (-0.205%)	0.4519 (-0.265%)	0.2891 (-0.310%)
$\mu = 1\,, l = 0$	0.6292 (-0.788%)	0.4487 (-0.971%)	0.2865 (-1.207%)
$\mu = 1.5\,, l = 0$	0.6225 (-1.845%)	0.4431 (-2.207%)	0.2823 (-2.655%)
$\mu = 2\,, l = 0$	0.6137 (-3.232%)	0.4359 (-3.796%)	0.2767 (-4.486%)
$\mu = 2.5\,, l = 0$	0.6039 (-4.778%)	0.4266 (-5.849%)	0.2696 (-7.034%)
$\mu = 3\,, l = 0$	0.5918 (-6.686%)	0.4170 (-7.967%)	0.2623 (-9.552%)
$\mu = 0\,, l = 0.5$	0.6355 (+0.205%)	0.4542 (+0.243%)	0.2909 (+0.310%)
$\mu = 0\,, l = 1$	0.6395 (+0.836%)	0.4576 (+0.993%)	0.2935 (+1.207%)
$\mu = 0\,, l = 1.5$	0.6461 (+1.883%)	0.4621 (+1.986%)	0.2979 (+2.724%)
$\mu = 0\,, l = 2$	0.6569 (+3.358%)	0.4705 (+3.840%)	0.3040 (+4.828%)
$\mu = 0\,, l = 2.5$	0.6665 (+5.093%)	0.4818 (+6.334%)	0.3115 (+7.414%)
$\mu = 0\,, l = 3$	0.6803 (+7.269%)	0.4926 (+8.718%)	0.3206 (+10.551%)

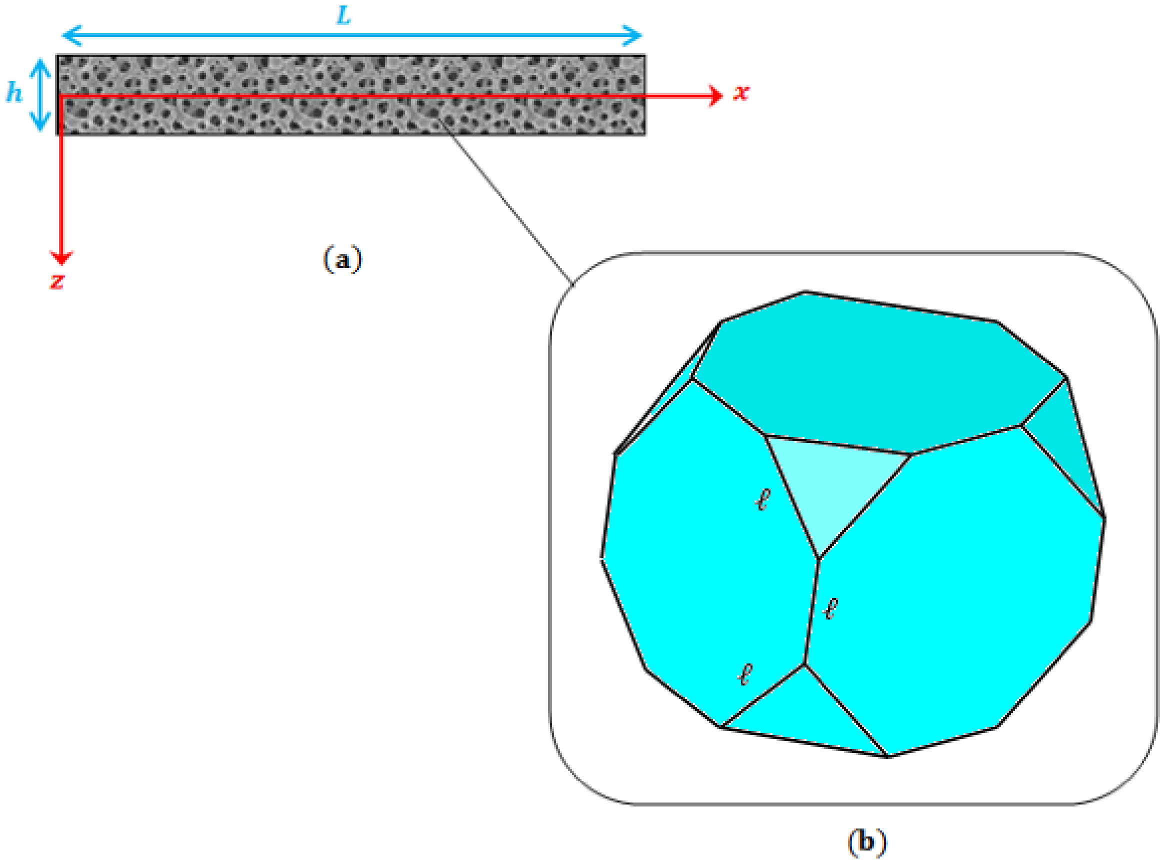

Figure 1: A micro/nano-beam made of a nanoporous biomaterial: (a) coordinate system and geometric parameters; (b) a truncated cube lattice framework including struts with length $\boldsymbol{\ell}$ and circular cross section of radius $\boldsymbol{r}$

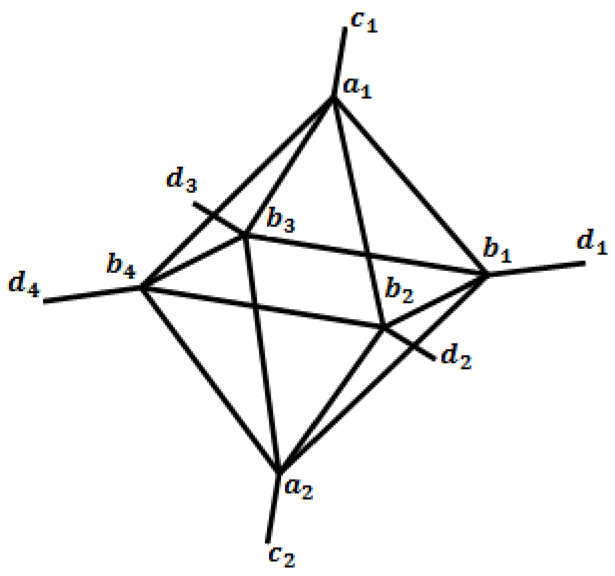

Figure 2: A schematic representation of a truncated cube unit cell

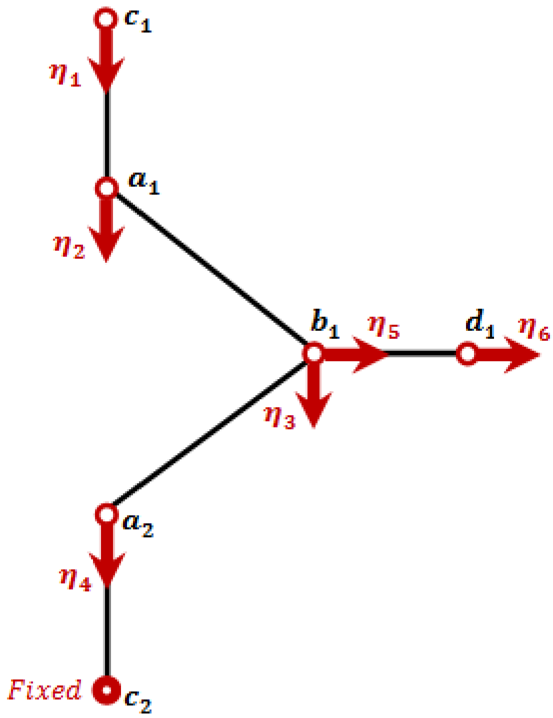

Figure 3: Degrees of freedom for the link $c_1a_1b_1d_1a_2c_2$ of the unit cell

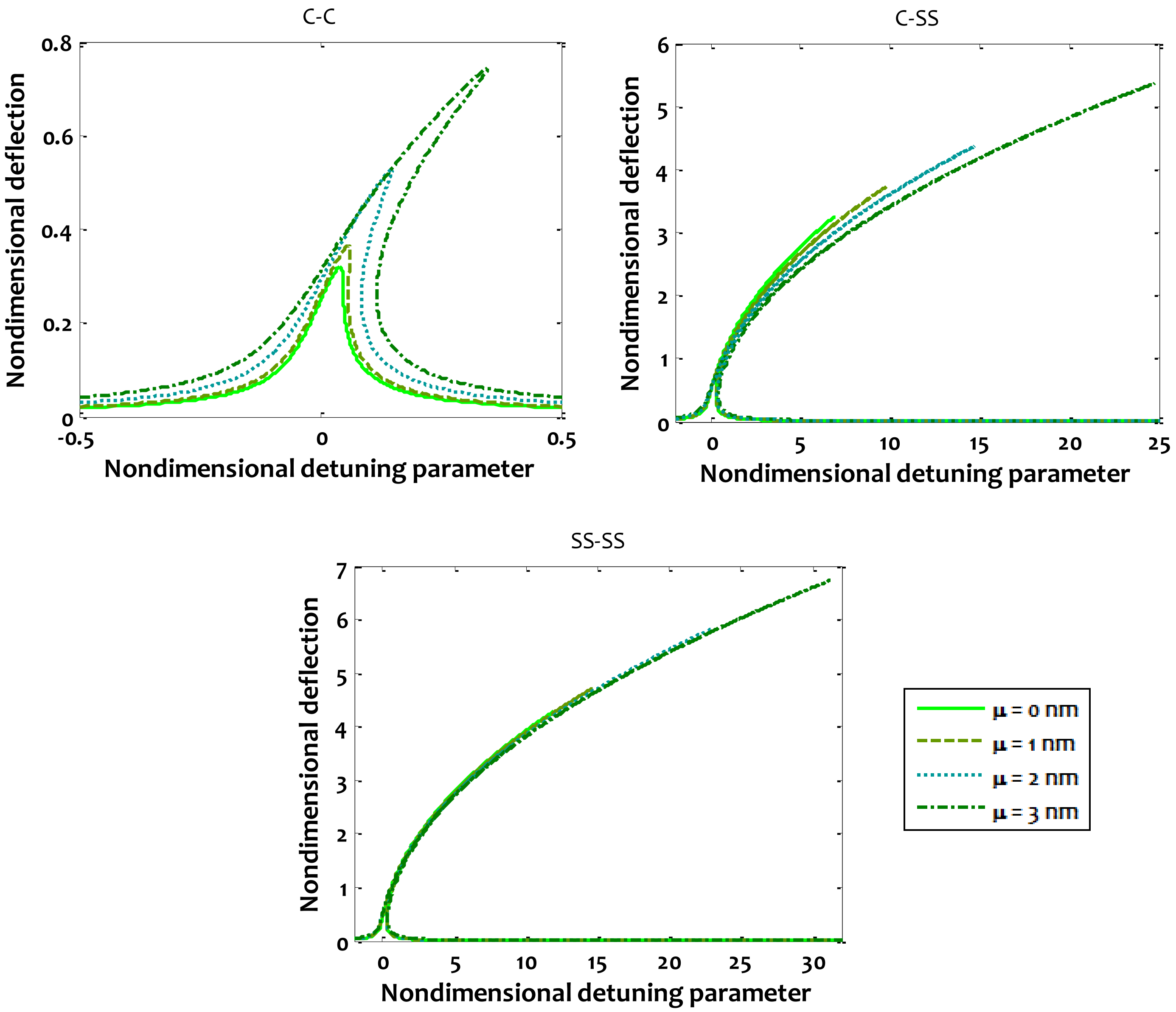

Figure 4: Size-dependent frequency-response of the micro/nano-beam under superharmonic excitation corresponding to different nonlocal parameters and boundary conditions ($l = 0\ nm$)

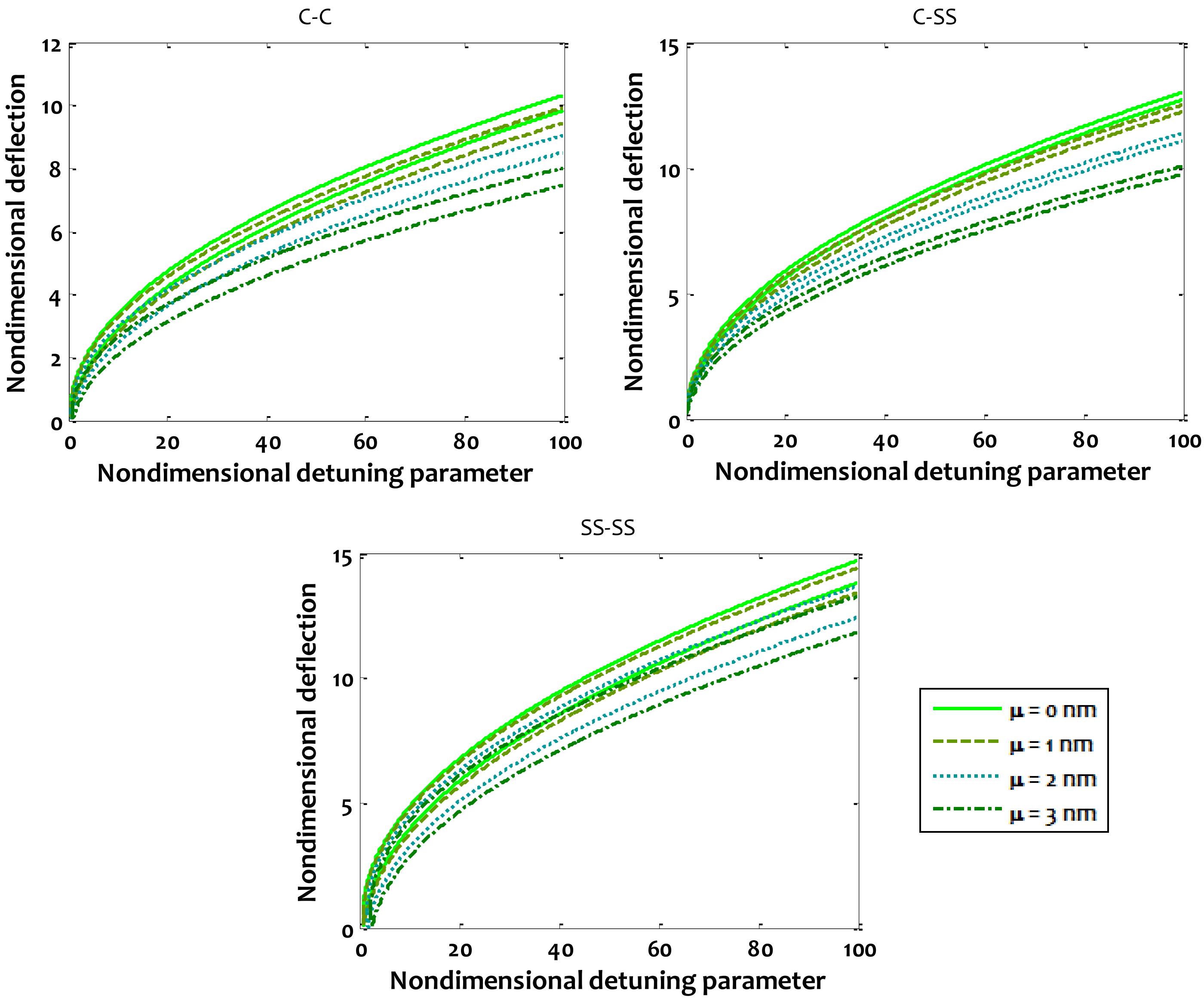

Figure 5: Size-dependent frequency-response of the micro/nano-beam under subharmonic excitation corresponding to different nonlocal parameters and boundary conditions ($l = 0\ nm$)

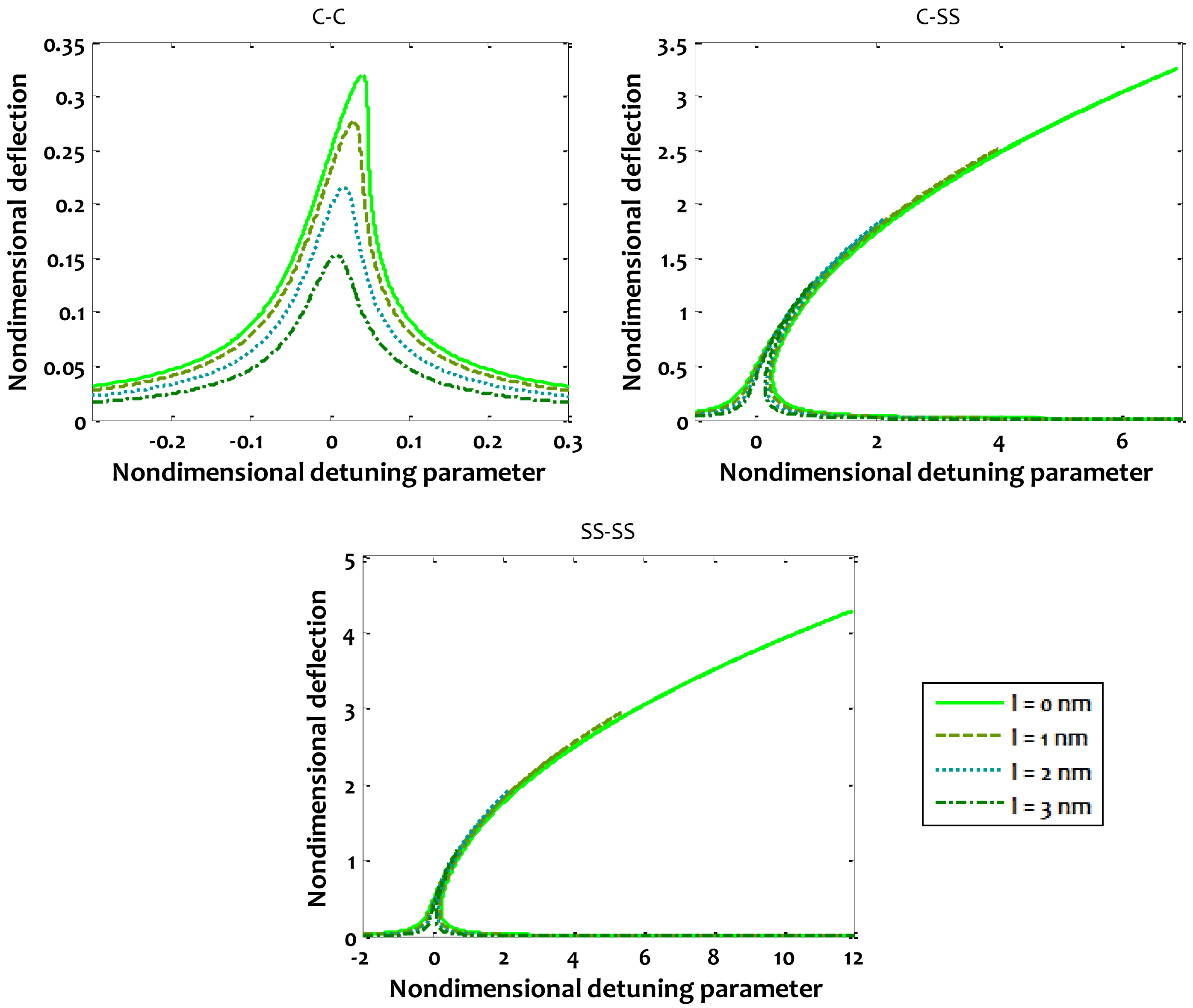

Figure 6: Size-dependent frequency-response of the micro/nano-beam under superharmonic excitation corresponding to different strain gradient parameters and boundary conditions ($\mu = 0\ nm$)

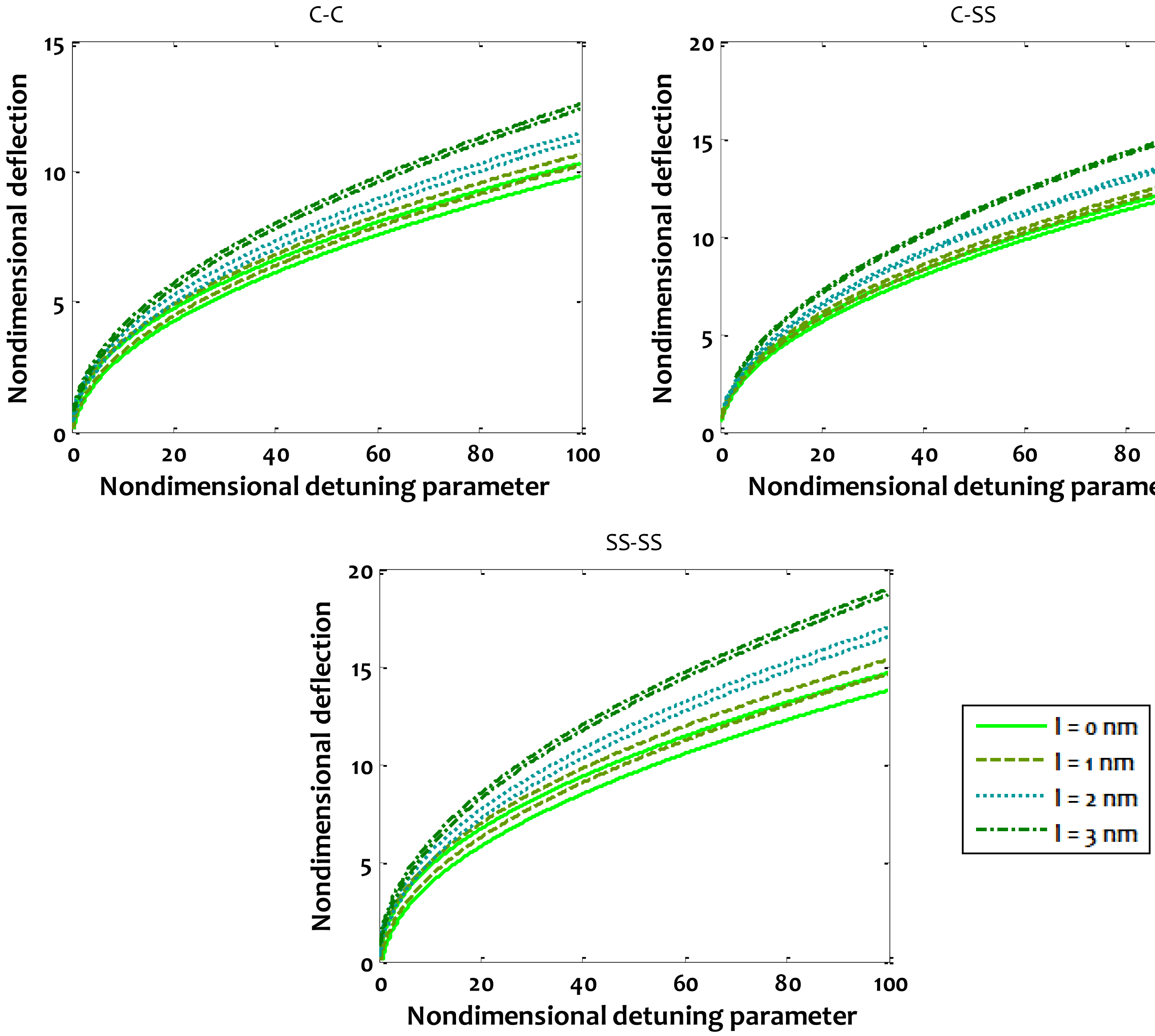

Figure 7: Size-dependent frequency-response of the micro/nano-beam under subharmonic excitation corresponding to different strain gradient parameters and boundary conditions ($\mu = 0\ nm$)

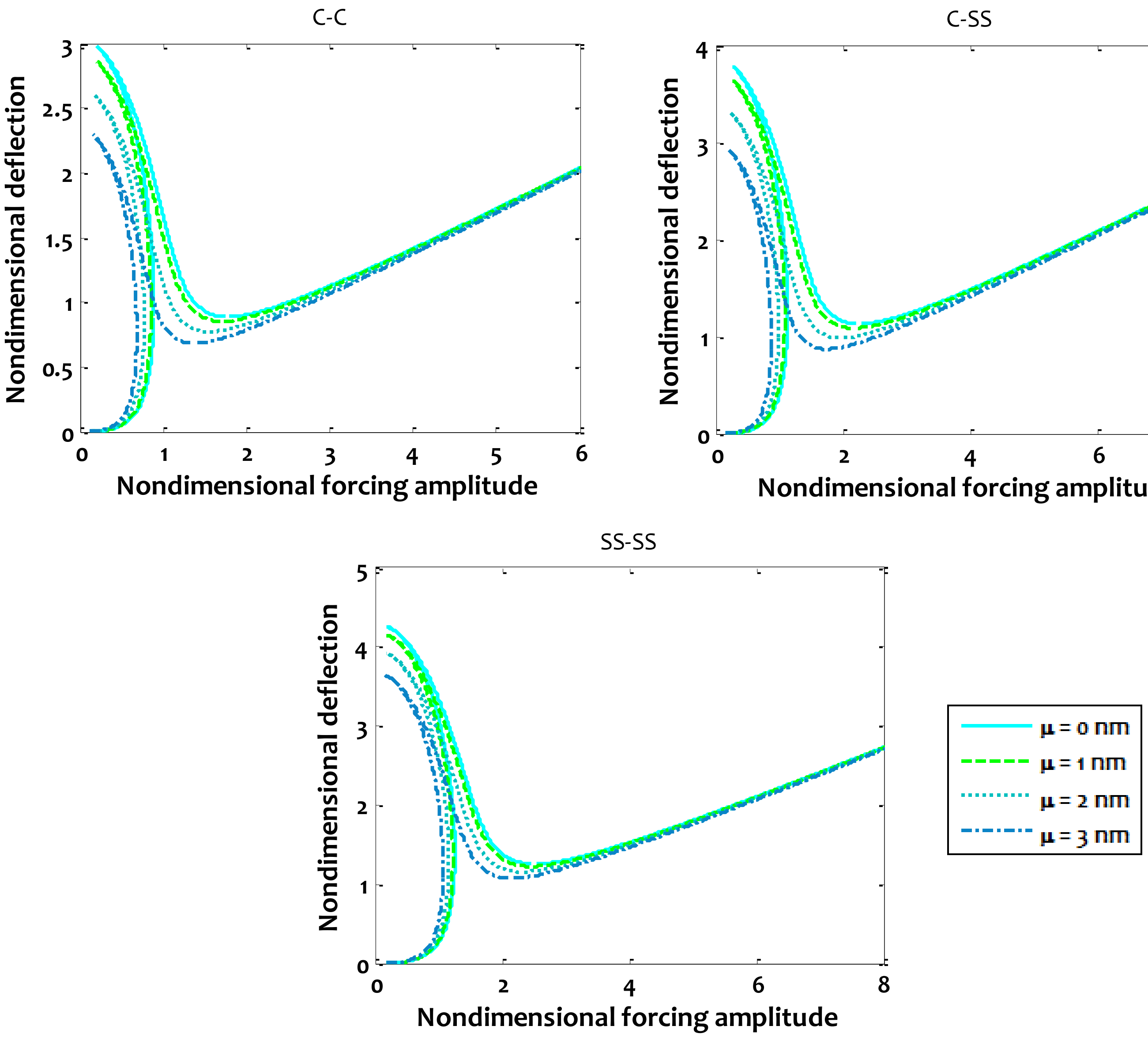

Figure 8: Size-dependent amplitude-response of the micro/nano-beam under superharmonic excitation corresponding to different nonlocal parameters and boundary conditions ($l = 0\ nm, \Gamma = 30$)

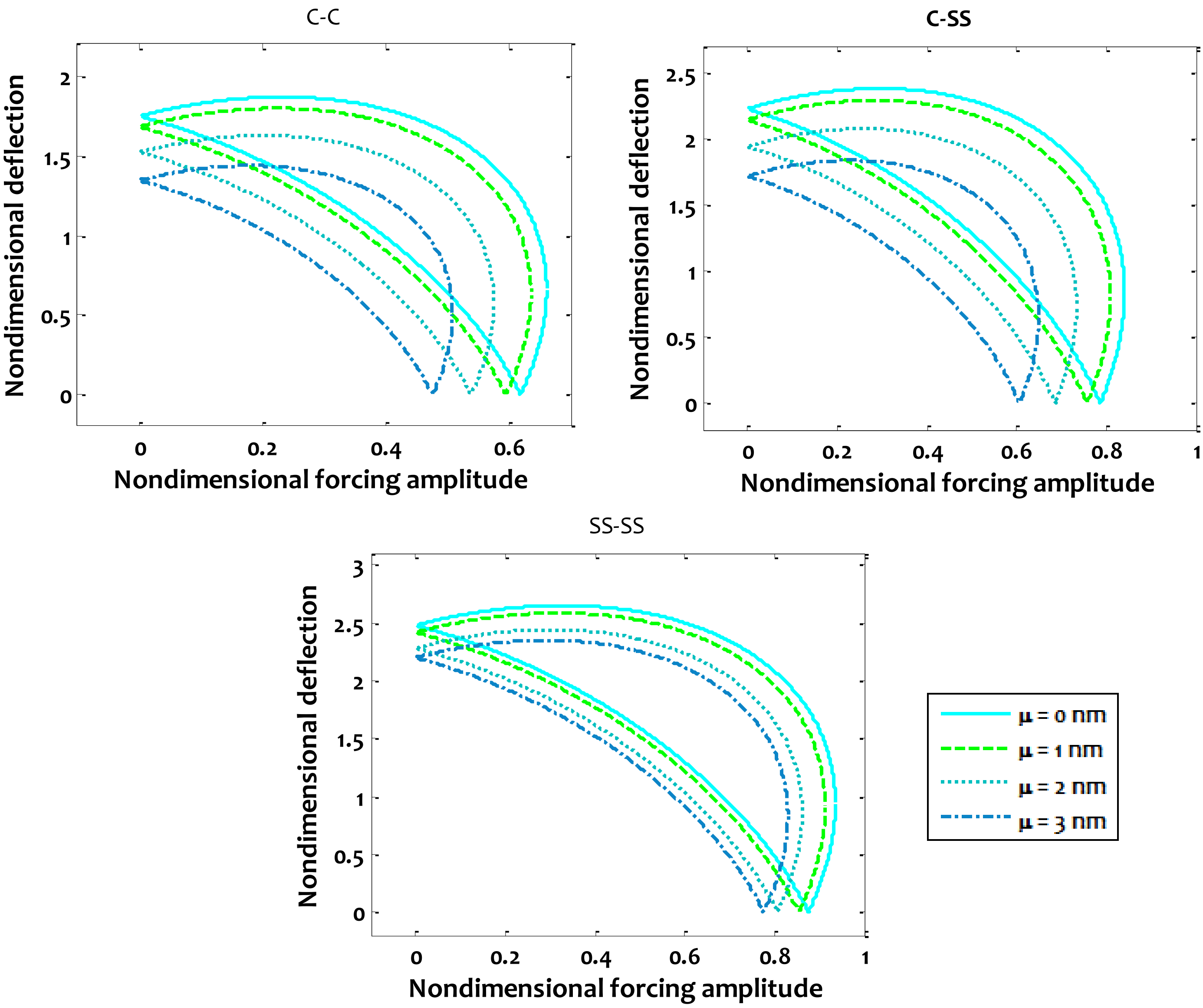

Figure 9: Size-dependent amplitude-response of the micro/nano-beam under subharmonic excitation corresponding to different nonlocal parameters and boundary conditions ($l = 0\ nm, \Gamma = 30$)

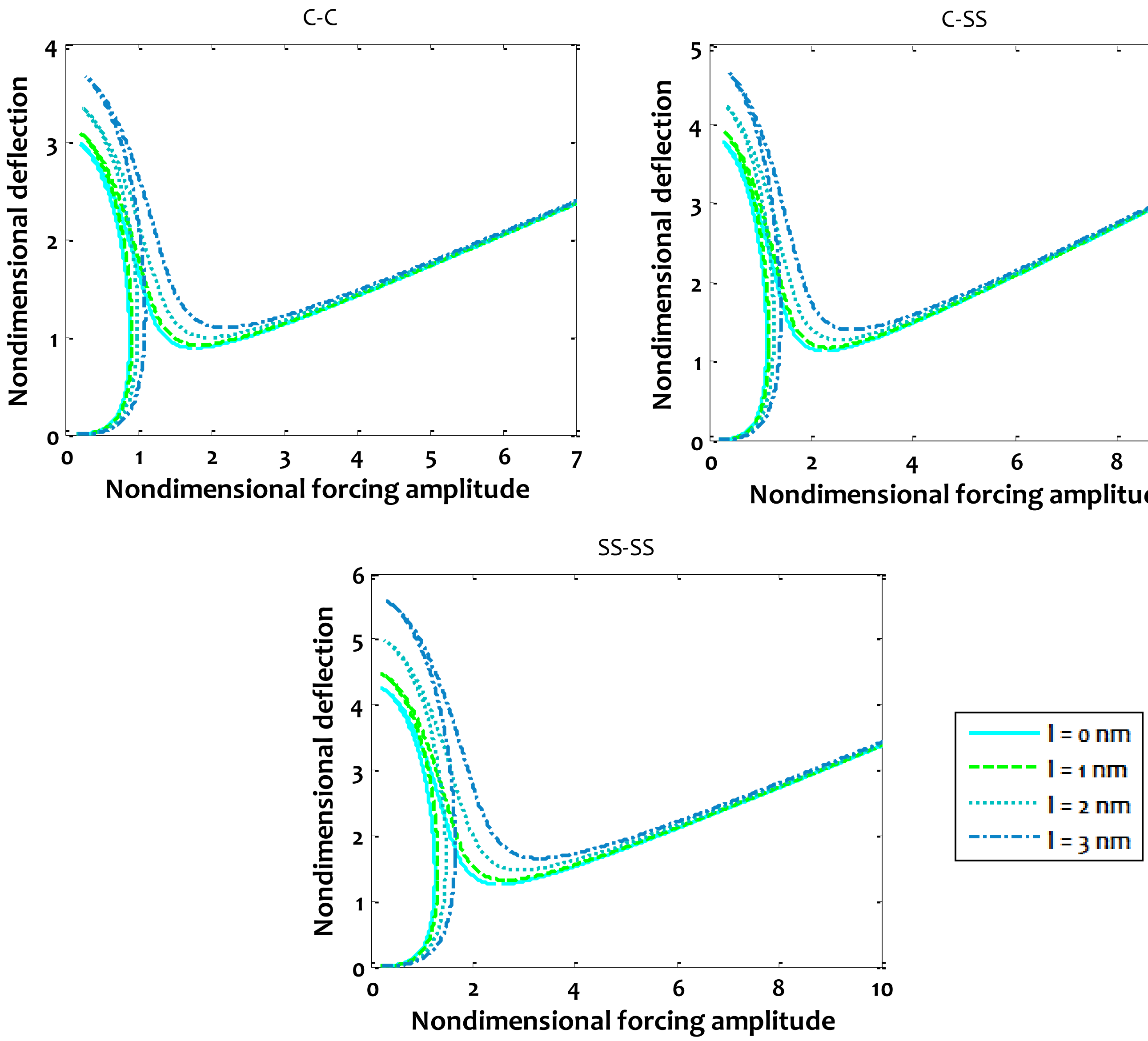

Figure 10: Size-dependent amplitude-response of the micro/nano-beam under superharmonic excitation corresponding to different strain gradient parameters and boundary conditions ($\mu = 0\ nm, \Gamma = 30$)

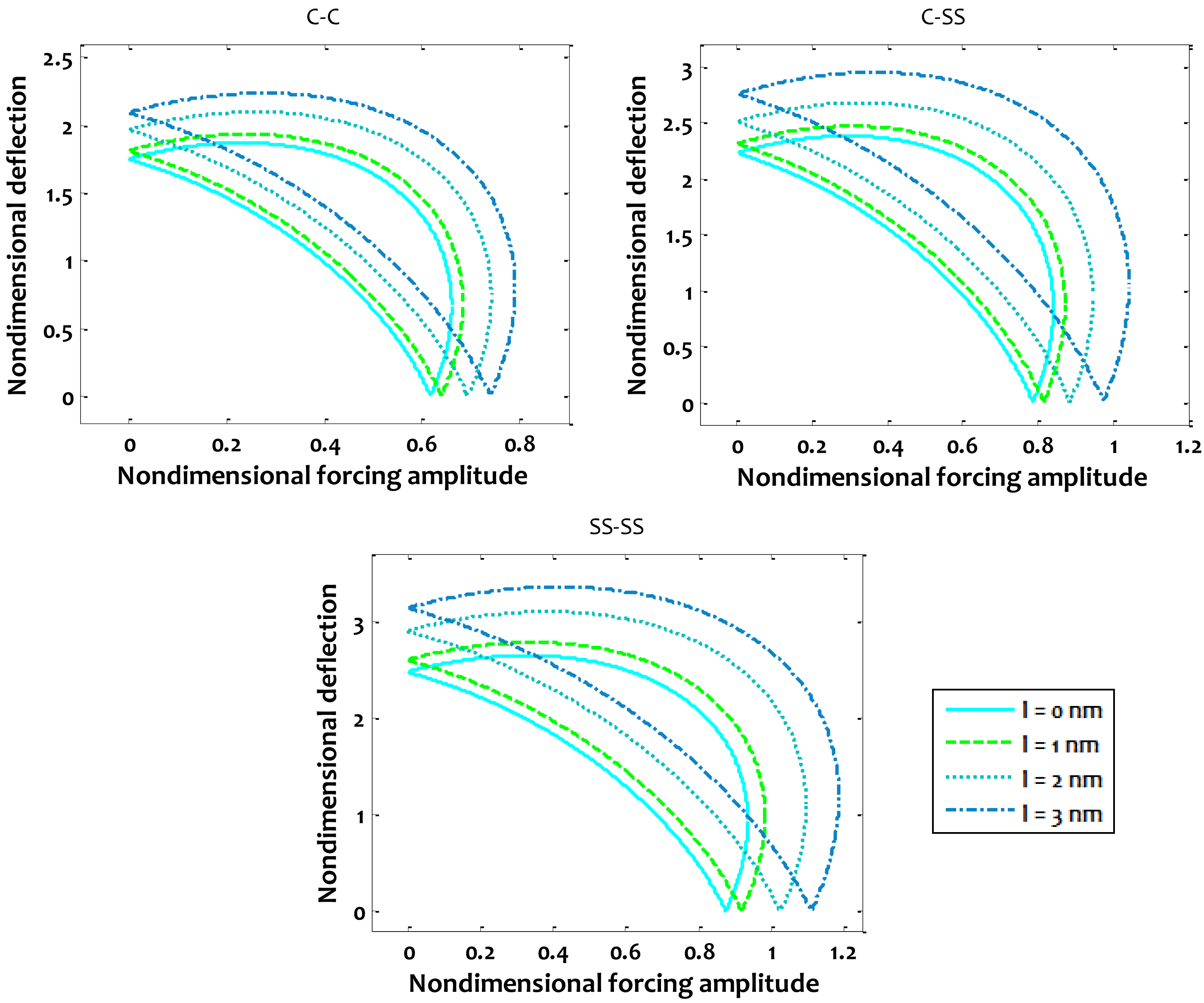

Figure 11: Size-dependent amplitude-response of the micro/nano-beam under subharmonic excitation corresponding to different strain gradient parameters and boundary conditions ($\mu = 0\ nm, \Gamma = 30$)

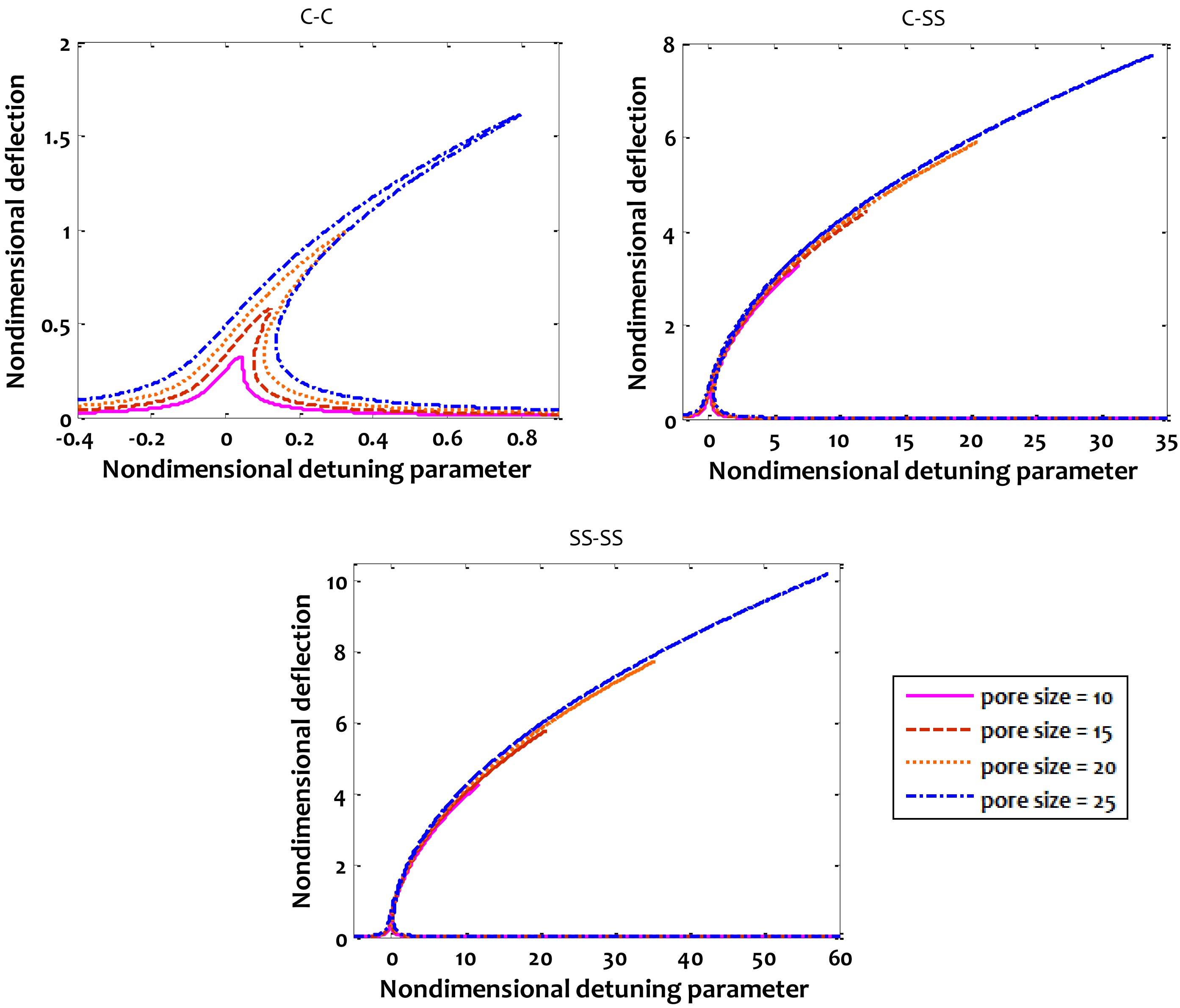

Figure 12: Influence of pore size on the size-dependent frequency-response of a micro/nano-beam made of nanoprous biomaterial under superharmonic excitation ($\mu = l = 1\ nm$)

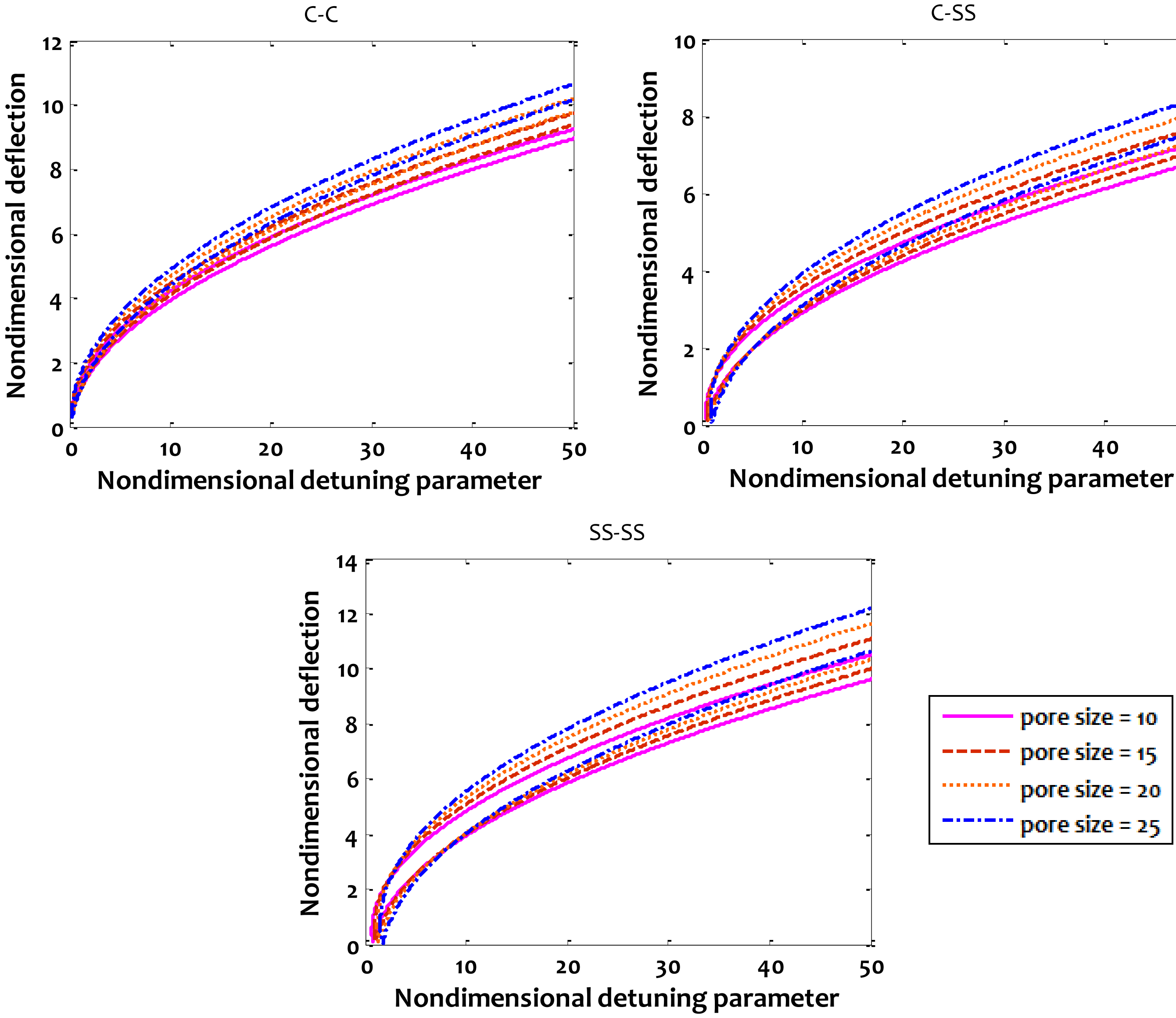

Figure 13: Influence of pore size on the size-dependent frequency-response of a micro/nano-beam made of nanoprous biomaterial under subharmonic excitation ($\mu = l = 1\ nm$)

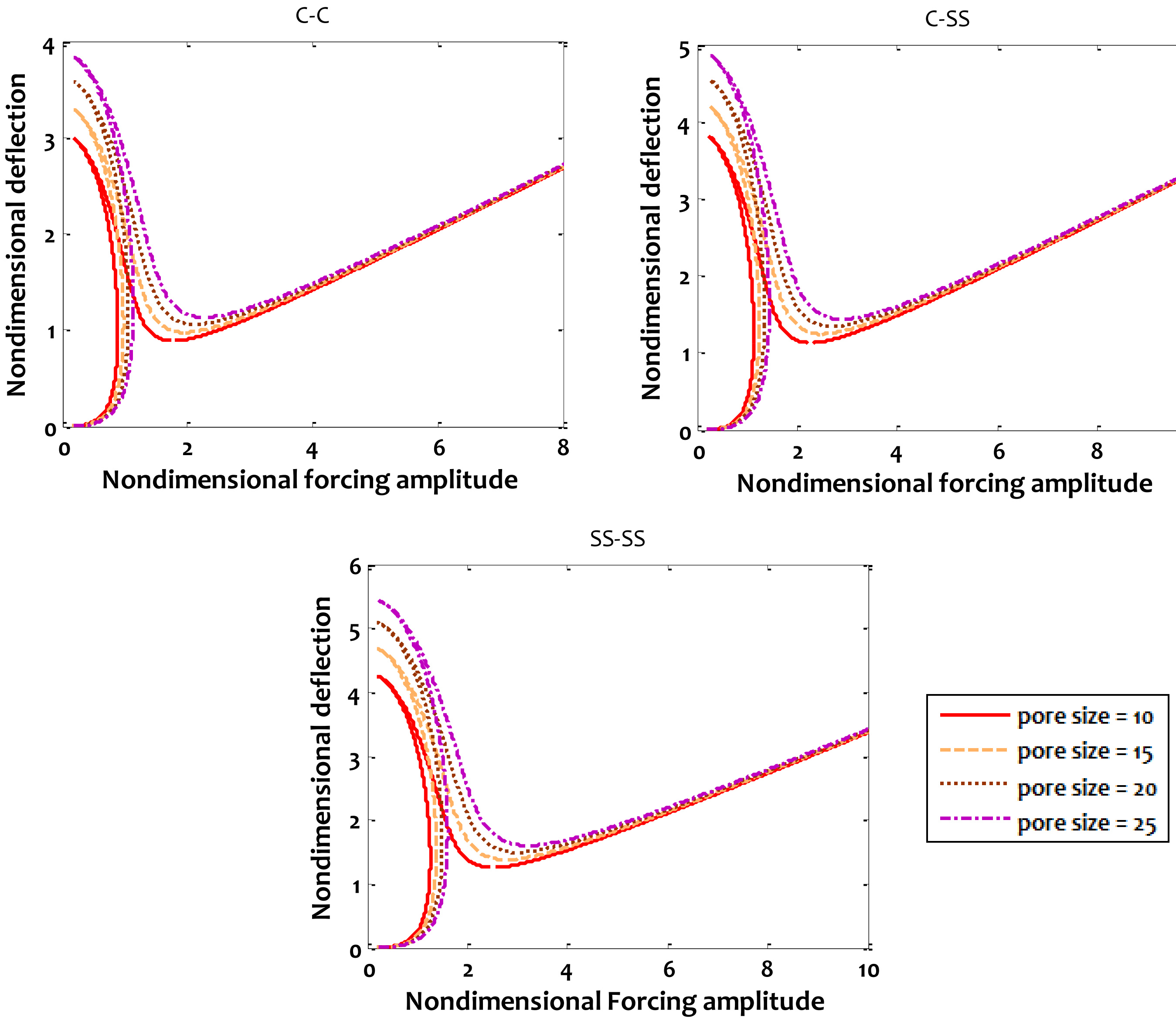

Figure 14: Influence of pore size on the size-dependent amplitude-response of a micro/nano-beam made of nanoprous biomaterial under superharmonic excitation ($\mu = l = 1\ nm, \Gamma = 30$)

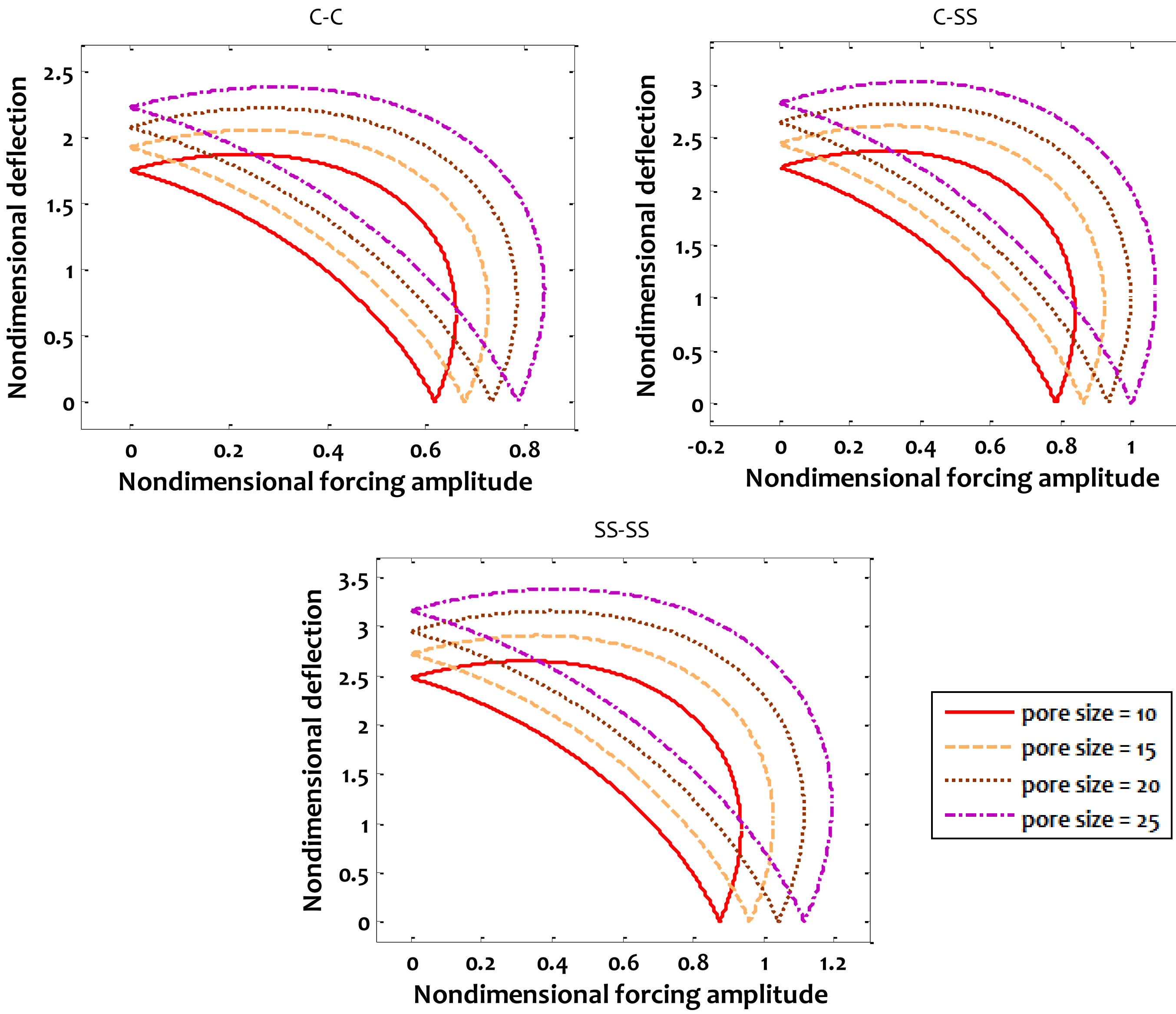

Figure 15: Influence of pore size on the size-dependent amplitude-response of a micro/nano-beam made of nanoprous biomaterial under subharmonic excitation ($\mu = l = 1\ nm, \Gamma = 30$)